Continuum Mech. Thermodyn.
https://doi.org/10.1007/s00161-021-01041-z

ORIGINAL ARTICLE

Santiago P. Clavijo · Luis Espath · Adel Sarmiento · Victor M. Calo

A continuum theory for mineral solid solutions undergoing chemo-mechanical processes

Received: 4 February 2021 / Accepted: 21 June 2021

Abstract Recent studies on metamorphic petrology as well as microstructural observations suggest the influence of mechanical effects upon chemically active metamorphic minerals. Thus, the understanding of such a coupling is crucial to describe the dynamics of geomaterials. In this effort, we derive a thermodynamically consistent framework to characterize the evolution of chemically active minerals. We model the metamorphic mineral assemblages as a solid-species solution where the species mass transport and chemical reaction drive the stress generation process. The theoretical foundations of the framework rely on modern continuum mechanics, thermodynamics far from equilibrium, and the phase-field model. We treat the mineral solid solution as a continuum body, and following the Larché and Cahn network model, we define displacement and strain fields. Consequently, we obtain a set of coupled chemo-mechanical equations. We use the aforementioned framework to study single minerals as solid solutions during metamorphism. Furthermore, we emphasise the use of the phase-field framework as a promising tool to model complex multi-physics processes in geoscience. Without loss of generality, we use common physical and chemical parameters found in the geoscience literature to portrait a comprehensive view of the underlying physics. Thereby, we carry out 2D and 3D numerical simulations using material parameters for mineral solid solutions to showcase and verify the chemo-mechanical interactions of mineral solid solutions that undergo spinodal decomposition, chemical reactions, and deformation.

Communicated by Andreas Öchsner.

S. P. Clavijo
Ali I. Al-Naimi Petroleum Engineering Research Center, King Abdullah University of Science and Technology (KAUST), Thuwal 23955-6900, Saudi Arabia

L. Espath
Department of Mathematics, RWTH Aachen University, Pontdriesch 14-16, 52062 Aachen, Germany
E-mail: espath@gmail.com

A. Sarmiento
Mathematics, Mechanics, and Materials Unit, Okinawa Institute of Science and Technology (OIST), 1919-1 Tancha, Onna, Kunigami District, Okinawa 904-0495, Japan

V. M. Calo
School of Earth and Planetary Sciences, Curtin University, Kent Street, Bentley, Perth, WA 6102, Australia

V. M. Calo
Curtin Institute for Computation, Curtin University, Kent Street, Bentley, Perth, WA 6102, Australia

V. M. Calo
Mineral Resources, Commonwealth Scientific and Industrial Research Organisation (CSIRO), 10 Kensington, Perth, WA 6152, Australia

Published online: 19 July 2021

Keywords Chemo-mechanics · Multicomponent · Cahn-Hilliard · Minerals · Metamorphism

1 Introduction

When considering a deformable medium, chemical reactions may affect the solid's strength and its mechanical properties. Analogously, high mechanical strength may restrict either the volumetric shrinkage or swelling[1] associated with the local volume changes caused by the chemical processes. Therefore, the chemical processes, associated with mass transport and chemical reactions, induce volume changes that lead to stresses around the reaction site.

Finding innovative ways of approaching the modeling of solids is an essential open research topic in science and engineering. For instance, areas such as material science and geoscience are continually searching for new models that allow to improve the properties of materials or to understand the formation of mineral assemblages, which directly relate to solids undergoing chemical processes. In particular, metamorphic petrologists report the reciprocal chemo-mechanical responses of minerals during metamorphism [1–7]. A variety of study cases of this coupling ranges from grain-scale pressure variations in high-temperature metamorphic rocks to the proper definition of pressure in order to define P/T conditions of mineral assemblages during a metamorphic cycle. Without loss of generality, we use the aforementioned framework to study the tempo-spatial variations of stress-assisted volume changes.

The description of solidity and its properties is crucial to describe the physical and chemical responses of solids accurately. Gibbs' comprehensive study set the foundations for the thermodynamical properties of solids [8]. However, Gibbs' solid model does not quantify the internal adjustment caused by compositional changes since the solid-state diffusion concept did not exist in his time. Herein, we seek to model multicomponent elastic solids that allow for changes in composition while remaining in the solid-state, and particularly, the impact of compositional changes on stress generation [9–12]. Larché and Cahn introduced the equilibrium conditions for deformable bodies, which change composition as a result of chemical processes [13–15]. For instance, dissolution and precipitation at solid-fluid interfaces change the chemical composition of the solid, which in turn induce stresses associated with volume changes. Larche-Cahn's approach models the solid as a network, which allows us to define the stress–strain relations. A solid network can be, for example, the unit cell of the crystalline structure of a mineral, which arranges the atoms in a systematic and repeating pattern. Thus, the network model of Larché and Cahn adequately describes a multicomponent solid.

The outline of this work is as follows. In Sect. 2, we present a detailed thermodynamically consistent treatment to the chemo-mechanical responses of the mineral solid solution. The chemo-mechanical framework relies on modern continuum mechanics, thermodynamics far from equilibrium, and the phase-field model. Sect. 3 covers the main results for the dimensionless coupled chemo-mechanical framework and the description of main equations and dimensionless vector and scalar numbers. Finally, in Sect. 4, we present 2D and 3D numerical simulations for ternary systems. Our simulation results portrait the interleaving between chemical and physical processes such as mass transport, chemical, interfacial effects and deformation. We also show the weak form of a finite element approach to solve the coupled systems of equations in their primal form.

2 Chemo-mechanical framework

2.1 Kinematics of motion

We propose a continuum framework to capture the evolution of a multicomponent elastic solid undergoing spinodal decomposition under multiple reversible chemical reactions. In our framework, the deformations induced across the solid boundaries and compositional changes drive the stress generation process. Henceforth, we refer to this mechanism as stress-assisted volume changes. Following the notation proposed by Fried and Gurtin [9], we treat the solid as a continuum body that occupies an open subset $\mathbf{B}$ of the Euclidean space $\mathcal{E}$. A time-dependent deformation field $\chi : \mathbf{B} \times]0, T[\rightarrow \mathcal{B}_t \subset \mathcal{E}$ describes the motion from a configuration $\mathbf{B}$ onto another configuration $\mathcal{B}_t$. We refer to $\mathbf{B}$ as the reference configuration and to $\mathbf{X}$ as the particles in $\mathbf{B}$. The reference configuration $\mathbf{B}$ represents an undeformed state of the solid. The deformation field characterizes the

[1] Thermal expansion and swelling phenomenon are unrelated. However, they produce the same mechanical effect. The swelling phenomenon produces changes in the hydrostatic part of the stress due to volumetric changes, which in turn are due to chemical processes.

kinematics of motion in the body, and after deformation, it assigns to each material particle $\mathbf{X}$ at a given $t \in \mathrm{T}$ a spatial particle $\mathbf{x}$ in the current configuration $\mathcal{B}_t$. Then, we express the deformation field as

$$\mathbf{x} \overset{\text{def}}{=} \boldsymbol{\chi}(\mathbf{X}, t) = \boldsymbol{\chi}_t(\mathbf{X}), \tag{1}$$

and abusing notation

$$\mathcal{B}_t = \boldsymbol{\chi}_t(\mathbf{B}). \tag{2}$$

The deformation field is invertible; namely, there exists an inverse deformation field $\boldsymbol{\chi}^{-1} : \mathcal{B}_t \times T \to \mathbf{B} \subset \mathcal{E}$ such that

$$\mathbf{x} = \boldsymbol{\chi}_t(\boldsymbol{\chi}^{-1}(\mathbf{x}, t)), \tag{3}$$

which renders

$$\mathbf{X} \overset{\text{def}}{=} \boldsymbol{\chi}^{-1}(\mathbf{x}, t). \tag{4}$$

2.2 Measure of strain

In deforming bodies undergoing mass transport and chemical reactions, the particles move relative to each other as a result of external forces and compositional changes. A description of this movement measures the relative displacement of the particles. We use a Lagrangian description of the displacement field $\mathbf{u}$ which defines the kinematics of the motion, that is,

$$\mathbf{u} = \mathbf{x}(\mathbf{X}, t) - \mathbf{X}, \tag{5}$$

and the deformation gradient

$$\mathbf{F} = \nabla \boldsymbol{\chi}_t = \nabla \mathbf{u} + \mathbf{I}, \tag{6}$$

where $\mathbf{I}$ denotes the second-order identity tensor. To ensure an admissible deformation, that is, a continuum body cannot penetrate itself, the Jacobian of the deformation gradient must fulfill the following constraint

$$J \overset{\text{def}}{=} \det \mathbf{F} > 0. \tag{7}$$

The velocity of a material particle $\mathbf{X}$ as a function of the motion is

$$\boldsymbol{V} \overset{\text{def}}{=} \frac{\partial \boldsymbol{\chi}(\mathbf{X}, t)}{\partial t}, \tag{8}$$

and its counterpart in the current configuration is

$$\boldsymbol{v} \overset{\text{def}}{=} \frac{\partial \boldsymbol{\chi}(\mathbf{X}, t)}{\partial t}\Big|_{\mathbf{X}=\boldsymbol{\chi}^{-1}(\mathbf{x},t)}. \tag{9}$$

Thus, the spatial velocity $\boldsymbol{v}$ describes a material particle located at $\mathbf{x} = \boldsymbol{\chi}_t(\mathbf{X})$ at time t.

Given the definition of the deformation gradient and the spatial velocity, the right Cauchy-Green stress, is given by

$$\mathbf{C} = \mathbf{F}^{\top}\mathbf{F}, \tag{10}$$

We apply the change of variables theorem to relate the reference and current configurations an infinitesimal area and volume elements, that is,

$$\mathrm{d}a = J\mathbf{F}^{-\top}\,\mathrm{d}a_{\mathrm{R}}, \tag{11}$$

$$\mathrm{d}v = J\,\mathrm{d}v_{\mathrm{R}}. \tag{12}$$

2.3 Fundamental balances

We derive a set of balance equations in the form of partial differential equations that define how the mass, linear and angular momenta, internal energy, and entropy vary in time as the solid-species system endures mechanical and chemical processes. As suggested in [9–12], three primary fields govern the coupled chemo-mechanical responses of the solid: the deformation $\boldsymbol{\chi}(\mathbf{X}, t)$, the species concentration $\varphi_{\mathrm{R}}^{\alpha}(\mathbf{X}, t)$ per unit of reference volume, and the chemical potential $\mu_{\mathrm{R}}^{\alpha}(\mathbf{X}, t)$ per unit of reference volume where α denotes the α-th species that composes the solid.

Let $\mathbf{P} \subset \mathbf{B}$ be an arbitrary control volume in conjunction with its boundary $\mathrm{S} = \partial\mathbf{P}$; analogously, consider $\mathcal{P}_t$ as a bounded control volume of $\mathcal{B}_t$ such that $\mathcal{P}_t = \boldsymbol{\chi}(\mathbf{P})$ with boundary $\mathcal{S} = \partial\mathcal{P}_t$. According to Cauchy's theorem, the traction $\mathbf{t}$ on a surface $\mathrm{d}a \subset \mathcal{S}$ and whose normal $\boldsymbol{n}$ points outwards is $\mathbf{t} = \mathbf{T}(\mathbf{x}, t)\boldsymbol{n}$, this traction characterizes the force exerted by the rest of the body $\mathcal{B}_t \setminus \mathcal{P}_t$ on $\mathcal{P}_t$ through $\mathrm{d}a \subset \mathcal{S}$ [10,11], where $\mathbf{t}$ depends linearly pointwise on the normal $\boldsymbol{n}$ through Cauchy's stress tensor $\mathbf{T}$ [16]. Applying (11) to the identity $\mathbf{t}_{\mathrm{R}}\,\mathrm{d}a_{\mathrm{R}} = \mathbf{t}\,\mathrm{d}a$, we find the force acting on the surface element $\mathrm{d}a$ as a function of the surface element $\mathrm{d}a_{\mathrm{R}}$ [9,10]. This identity leads to the nominal stress tensor $\mathbf{T}_{\mathrm{R}}$, that is, the first Piola-Kirchhoff,

$$\mathbf{T}_{\mathrm{R}}\mathbf{N}\,\mathrm{d}a_{\mathrm{R}} = \mathbf{T}\boldsymbol{n}\,\mathrm{d}a \quad \text{with} \quad \mathbf{T}_{\mathrm{R}} = J\mathbf{T}\mathbf{F}^{-\top}. \tag{13}$$

As mentioned above, the chemo-mechanical interactions take place through an elastically deforming solid composed by a network and constituent species. Consequently, we formulate balances of mass conservation for both the solid and the constituent species. Thus, we define $\varphi_{\mathrm{R}}^{\alpha}$ as the local concentration of the α-th species per unit of undeformed configuration together with a spatial species outflux $\boldsymbol{\jmath}^{\alpha}$. In agreement with the balance of mass conservation, the rate of mass change of the α-th species in the control volume $\mathbf{P}$ has to be equal to the contribution from the mass supply, typically caused by chemical reactions between the species, and the net mass flux through the boundary $\mathcal{S}$, that is,

$$\overline{\int_{\mathbf{P}} \varphi_{\mathrm{R}}^{\alpha}\,\mathrm{d}v_{\mathrm{R}}}^{\cdot} = \int_{\mathbf{P}} s^{\alpha}\,\mathrm{d}v_{\mathrm{R}} - \int_{\mathcal{S}} \boldsymbol{\jmath}^{\alpha}\cdot\boldsymbol{n}\,\mathrm{d}a, \tag{14}$$

where s^{α} is the mass supply expressed in the reference configuration. The mass supply is composed of two terms, an external contribution due to external agents and internal contributions caused by chemical reactions. Thereby,

$$s^{\alpha} = s^{\alpha}_{\mathrm{int}} + s^{\alpha}_{\mathrm{ext}}. \tag{15}$$

Using the divergence theorem, we transform the surface integral of the species flux into a volume integral of the divergence of the species flux as follows

$$\overline{\int_{\mathbf{P}} \varphi_{\mathrm{R}}^{\alpha}\,\mathrm{d}v_{\mathrm{R}}}^{\cdot} = \int_{\mathbf{P}} s^{\alpha}\,\mathrm{d}v_{\mathrm{R}} - \int_{\mathcal{P}_t} \operatorname{div}\boldsymbol{\jmath}^{\alpha}\,\mathrm{d}v. \tag{16}$$

The Lagrangian description of (16) is

$$\overline{\int_{\mathbf{P}} \varphi_{\mathrm{R}}^{\alpha}\,\mathrm{d}v_{\mathrm{R}}}^{\cdot} = \int_{\mathbf{P}} s^{\alpha}\,\mathrm{d}v_{\mathrm{R}} - \int_{\mathbf{P}} \operatorname{Div}\boldsymbol{\jmath}_{\mathrm{R}}^{\alpha}\,\mathrm{d}v_{\mathrm{R}}, \tag{17}$$

where we use the Piola transform. Thus, the material species flux is then $\boldsymbol{\jmath}_{\mathrm{R}}^{\alpha} = \mathbf{F}^{-1}(J\boldsymbol{\jmath}^{\alpha})$. Finally, the localized version of (17) is

$$\dot{\varphi}_{\mathrm{R}}^{\alpha} = s^{\alpha} - \operatorname{Div}\boldsymbol{\jmath}_{\mathrm{R}}^{\alpha}. \tag{18}$$

The concentration of each species is linearly dependent on the other, via the following constraint,

$$\sum_{\alpha=1}^{n} \varphi_{\mathrm{R}}^{\alpha} = 1, \tag{19}$$

which renders

$$\sum_{\alpha=1}^{n} \dot{\varphi}_{\mathrm{R}}^{\alpha} = 0 \;\text{ and }\; \sum_{\alpha=1}^{n} \nabla\varphi_{\mathrm{R}}^{\alpha} = 0, \tag{20}$$

where n stands for the total number of species. The mass constraint that (19) expresses must hold when the solid is solely composed of the diffusing species. Herein, we restrict our attention to the case where mass transport by vacancies is not feasible.

Henceforth, a superimposed dot ($\dot{\ }$) stands for the material time derivative, for instance, $\dot{\varphi}^{\alpha}_{\mathrm{R}}$ is the material time derivative of the concentration species. Given the conservation of the solid mass, we define ρ and ρ_0 as the solid density in the current and reference configuration, respectively. Then, the balance of solid mass reads

$$\int_{\mathcal{P}_t} \rho \, \mathrm{d}v = \int_{\mathbf{P}} \rho_0 \, \mathrm{d}v_{\mathrm{R}}, \tag{21}$$

In (21), we convert the volume integral in the current configuration into its counterpart in the reference configuration by employing the relation (12). Finally, we use the localization theorem that leads to the local conservation of solid mass

$$\rho_0 = J\rho. \tag{22}$$

Neglecting all inertial effects to focus on quasi-static processes, i.e., we assume the spatial velocity $\boldsymbol{v}$ is nearly constant through the time, the balance of conservation of linear momentum reads

$$\int_{\mathcal{S}} \boldsymbol{t} \, \mathrm{d}a + \int_{\mathbf{P}} \mathbf{b} \, \mathrm{d}v_{\mathrm{R}} = \mathbf{0}. \tag{23}$$

The balance of linear momentum relates forces to changes in the motion of the body. Such balance involves the traction $\mathbf{t}$ acting on a surface element $\mathrm{d}a$ as well as a body force $\mathbf{b}$. Conventionally, the body force $\mathbf{b}$ accounts for forces resulting from gravitational effects. Through the divergence theorem, we express the surface integral in (23) as a volume integral

$$\int_{\mathcal{P}_t} \operatorname{div} \mathbf{T} \, \mathrm{d}v + \int_{\mathbf{P}} \mathbf{b} \, \mathrm{d}v_{\mathrm{R}} = \mathbf{0}, \tag{24}$$

and after some straightforward manipulations in (24), the localized Lagrangian form of the balance of linear momentum is

$$\operatorname{Div} \mathbf{T}_{\mathrm{R}} + \mathbf{b} = \mathbf{0}. \tag{25}$$

The balance of conservation of angular momentum is

$$\int_{\mathcal{P}_t} \mathbf{x} \times \boldsymbol{t} \, \mathrm{d}v + \int_{\mathbf{P}} \mathbf{x} \times \mathbf{b} \, \mathrm{d}v_{\mathrm{R}} = \mathbf{0}. \tag{26}$$

After using the definition of the balance of linear momentum, the divergence theorem, and the localization theorem, this implies that $\mathbf{T}^{\top} = \mathbf{T}$. The previous relation implies the symmetry of the Cauchy's tensor [17,18]. Finally, the localized Lagrangian form of the balance of angular momenta is

$$\operatorname{skw} \mathbf{T}_{\mathrm{R}} \mathbf{F}^{\top} = \mathbf{0}. \tag{27}$$

Following the line of thought introduced by Gurtin and Fried [19–22], we separate balances of conservation laws from constitutive equations. As a consequence, we include a balance of microforces, that is

$$\int_{\mathbf{P}} (\pi^{\alpha} + \gamma^{\alpha}) \, \mathrm{d}v_{\mathrm{R}} = -\int_{\mathcal{S}} \boldsymbol{\xi}^{\alpha} \cdot \boldsymbol{n} \, \mathrm{d}a, \tag{28}$$

where the vector $\boldsymbol{\xi}^{\alpha}$ and the scalar π^{α} (γ^{α}) correspond to the α-th microstress and α-th the internal (external) microforce, respectively. In general, the microstresses and microforces are quantities associated with the microscopic configuration of atoms. We express the microforce balances in a Lagrangian form

$$\int_{\mathbf{P}} (\pi^{\alpha} + \gamma^{\alpha}) \, \mathrm{d}v_{\mathrm{R}} = -\int_{\mathbf{P}} \operatorname{Div} \boldsymbol{\xi}^{\alpha}_{\mathrm{R}} \, \mathrm{d}v_{\mathrm{R}}, \tag{29}$$

and after applying the locatization theorem, the microforce balances read

$$\pi^{\alpha} + \gamma^{\alpha} = -\operatorname{Div} \boldsymbol{\xi}^{\alpha}_{\mathrm{R}}, \tag{30}$$

where $\boldsymbol{\xi}^{\alpha}_{\mathrm{R}} = \mathbf{F}^{-1}(J\boldsymbol{\xi}^{\alpha})$.

2.4 Laws of thermodynamics and free-energy inequality

To describe the thermodynamics of this system, we introduce a power expenditure $\mathcal{W}_{\text{ext}} = \mathcal{W}_{\text{ext}}(\mathbf{P}) + \mathcal{W}_{\text{ext}}(\mathcal{P})$ externally to $\mathbf{P}$ and $\mathcal{P}$ done by the external microforce and force on $\mathbf{P}$, and the microtraction and traction on $\mathcal{S}$

$$\mathcal{W}_{\text{ext}}(\mathbf{P}) = \sum_{\alpha=1}^{n} \left\{ \int_{\mathbf{P}} \gamma^{\alpha} \dot{\varphi}_{\text{R}}^{\alpha} \, \mathrm{d}v_{\text{R}} \right\} + \int_{\mathbf{P}} \mathbf{b} \cdot \boldsymbol{v} \, \mathrm{d}v_{\text{R}}, \tag{31a}$$

$$\mathcal{W}_{\text{ext}}(\mathcal{P}) = \sum_{\alpha=1}^{n} \left\{ \int_{\mathcal{S}} \xi_{\mathcal{S}}^{\alpha} \dot{\varphi}_{\text{R}}^{\alpha} \, \mathrm{d}a \right\} + \int_{\mathcal{S}} \boldsymbol{t} \cdot \boldsymbol{v} \, \mathrm{d}a. \tag{31b}$$

By neglecting all inertial effects and body forces, we use the first law of thermodynamics to characterize the balance between the rate of internal energy $\dot{\varepsilon}$ and the expenditure rate of the chemo-mechanical power, caused by external forces, species transport, and chemical reactions. The first law is then,

$$\dot{\overline{\int_{\mathbf{P}} \varepsilon \, \mathrm{d}v_{\text{R}}}} = \mathcal{W}_{\text{ext}} - \int_{\mathcal{S}} \boldsymbol{q} \cdot \boldsymbol{n} \, \mathrm{d}a + \int_{\mathbf{P}} r \, \mathrm{d}v_{\text{R}} - \sum_{\alpha=1}^{n} \left\{ \int_{\mathcal{S}} \mu_{\text{R}}^{\alpha} \boldsymbol{J}^{\alpha} \cdot \boldsymbol{n} \, \mathrm{d}a - \int_{\mathbf{P}} \mu_{\text{R}}^{\alpha} s_{\text{ext}}^{\alpha} \, \mathrm{d}v_{\text{R}} \right\}. \tag{32}$$

There is no contribution of s_{int}^{α} to the energy balance (32). The entropy imbalance, in the form of the Clausius–Duhem inequality, states that the rate of growth of the entropy η is at least as large as the entropy flux $\boldsymbol{q}/\vartheta$ plus the contribution from the entropy supply q/ϑ, that is,

$$\dot{\overline{\int_{\mathbf{P}} \eta \, \mathrm{d}v_{\text{R}}}} \geq - \int_{\mathcal{S}} \frac{\boldsymbol{q} \cdot \boldsymbol{n}}{\vartheta} \, \mathrm{d}a + \int_{\mathbf{P}} \frac{r}{\vartheta} \, \mathrm{d}v_{\text{R}}, \tag{33}$$

where $\boldsymbol{q}$, r, and ϑ stand for the spatial heat flux, heat supply, and temperature, respectively. The localized Lagrangian version of (32) and (33) read

$$\dot{\varepsilon} = \mathcal{W}_{\text{ext}} - \operatorname{Div} \boldsymbol{q}_{\text{R}} + r - \sum_{\alpha=1}^{n} \left\{ \operatorname{Div} \mu_{\text{R}}^{\alpha} \boldsymbol{J}_{\text{R}}^{\alpha} - \mu_{\text{R}}^{\alpha} s_{\text{ext}}^{\alpha} \right\}, \tag{34}$$

and

$$\dot{\eta} \geq -\operatorname{Div} \vartheta^{-1} \boldsymbol{q}_{\text{R}} + \vartheta^{-1} r, \tag{35}$$

where $\boldsymbol{q}_{\text{R}} = \mathbf{F}^{-1}(J\boldsymbol{q})$ is the material heat flux. Moreover, $\mathcal{W}_{\text{ext}}$ is

$$\mathcal{W}_{\text{ext}} = \sum_{\alpha=1}^{n} \left\{ (\operatorname{Div} \boldsymbol{\xi}_{\text{R}}^{\alpha} + \gamma^{\alpha}) \dot{\varphi}_{\text{R}}^{\alpha} + \boldsymbol{\xi}_{\text{R}}^{\alpha} \cdot \nabla \dot{\varphi}_{\text{R}}^{\alpha} \right\} + (\operatorname{Div} \mathbf{T}_{\text{R}} + \mathbf{b}) \cdot \boldsymbol{v} + \mathbf{T}_{\text{R}} : \dot{\mathbf{F}}. \tag{36}$$

Rewriting (34) and (35), and multiplying (35) by ϑ, we obtain

$$\dot{\varepsilon} = \mathcal{W}_{\text{ext}} - \operatorname{Div} \boldsymbol{q}_{\text{R}} + r - \sum_{\alpha=1}^{n} \left\{ \nabla \mu_{\text{R}}^{\alpha} \cdot \boldsymbol{J}_{\text{R}}^{\alpha} + \mu_{\text{R}}^{\alpha} \operatorname{Div} \boldsymbol{J}_{\text{R}}^{\alpha} - \mu_{\text{R}}^{\alpha} s_{\text{ext}}^{\alpha} \right\}, \tag{37}$$

and

$$\vartheta \dot{\eta} \geq \vartheta^{-1} \nabla \vartheta \cdot \boldsymbol{q}_{\text{R}} - \operatorname{Div} \boldsymbol{q}_{\text{R}} + r. \tag{38}$$

We obtain Helmholtz free energy from applying the Legendre transform to the internal energy while replacing the entropy of the system by the temperature as an independent variable., i.e., $\dot{\psi} = \dot{\varepsilon} - \dot{\vartheta}\eta - \vartheta\dot{\eta}$. Consequently, we obtain

$$\dot{\psi} \leq \mathcal{W}_{\text{ext}} - \sum_{\alpha=1}^{n} \left\{ \nabla \mu_{\text{R}}^{\alpha} \cdot \boldsymbol{J}_{\text{R}}^{\alpha} + \mu_{\text{R}}^{\alpha} \operatorname{Div} \boldsymbol{J}_{\text{R}}^{\alpha} - \mu_{\text{R}}^{\alpha} s_{\text{ext}}^{\alpha} \right\} - \vartheta^{-1} \nabla \vartheta \cdot \boldsymbol{q}_{\text{R}} - \dot{\vartheta} \eta, \tag{39}$$

Introducing the balances of both mass conservation and microforces into (39), the free-energy inequality under isothermal conditions is

$$\dot{\psi} \leq \mathbf{T}_{\text{R}} : \dot{\mathbf{F}} + \sum_{\alpha=1}^{n} \left\{ (\mu_{\text{R}}^{\alpha} - \pi^{\alpha}) \dot{\varphi_{\text{R}}^{\alpha}} + \boldsymbol{\xi}_{\text{R}}^{\alpha} \cdot \nabla \dot{\varphi_{\text{R}}^{\alpha}} - \boldsymbol{J}_{\text{R}}^{\alpha} \cdot \nabla \mu_{\text{R}}^{\alpha} - \mu_{\text{R}}^{\alpha} s_{\text{int}}^{\alpha} \right\}. \tag{40}$$

2.5 The principle of material frame indifference

Throughout the derivation of the constitutive behavior of the multicomponent solid, we use the Larché–Cahn derivative for both scalar and gradient fields as expressed by [23], together with the mass constraint given by (19). We assume the following constitutive dependence of the free energy ψ

$$\psi = \hat{\psi}(\boldsymbol{\varphi}_{\mathrm{R}}, \nabla\boldsymbol{\varphi}_{\mathrm{R}}, \mathbf{F}) = \hat{\psi}^{ch}(\boldsymbol{\varphi}_{\mathrm{R}}, \nabla\boldsymbol{\varphi}_{\mathrm{R}}) + \hat{\psi}^{el}(\mathbf{F}^{e}(\mathbf{F}, \boldsymbol{\varphi}_{\mathrm{R}})). \tag{41}$$

The objectivity principle requires the constitutive relation (41) to be invariant under a superposed rigid body motion or equivalently, independent of the observer. We can relate two different displacement fields χ and χ^{*} as follows

$$\chi^{*}(\mathbf{X}, t) = \mathbf{Q}(t)\chi(\mathbf{X}, t) + \mathbf{c}(t), \tag{42}$$

where $\mathbf{Q}(t)$ represents a rotation tensor and $\mathbf{c}(t)$ the relative translations. Therefore, the transformation of the potential (41) following (42) implies

$$\psi = \hat{\psi}(\boldsymbol{\varphi}_{\mathrm{R}}, \nabla\boldsymbol{\varphi}_{\mathrm{R}}, \mathbf{F}) = \overline{\psi}(\boldsymbol{\varphi}_{\mathrm{R}}, \nabla\boldsymbol{\varphi}_{\mathrm{R}}, \mathbf{C}), \tag{43}$$

which ensures consistency with the dissipation inequality (40) and the principle of frame-indifference.

2.6 Constitutive equations

By using the Coleman-Noll procedure [24], we find a set of constitutive equations as a pair for each kinematic process. We then rewrite (40) following 41 as

$$\left(\mathbf{T}_{\mathrm{R}} - \frac{\partial\hat{\psi}}{\partial\mathbf{F}}\right) : \dot{\mathbf{F}} + \sum_{\alpha=1}^{n}\left(\mu_{\mathrm{R}}^{\alpha} - \pi^{\alpha} - \frac{\partial\hat{\psi}}{\partial\varphi_{\mathrm{R}}^{\alpha}}\right)\dot{\varphi}_{\mathrm{R}}^{\alpha} + \sum_{\alpha=1}^{n}\left(\boldsymbol{\xi}_{\mathrm{R}}^{\alpha} - \frac{\partial\hat{\psi}}{\partial\nabla\varphi_{\mathrm{R}}^{\alpha}}\right)\cdot\nabla\dot{\varphi}_{\mathrm{R}}^{\alpha} - \sum_{\alpha=1}^{n}\left\{\boldsymbol{J}_{\mathrm{R}}^{\alpha}\cdot\nabla\mu_{\mathrm{R}}^{\alpha} + \mu_{\mathrm{R}}^{\alpha}s_{\mathrm{int}}^{\alpha}\right\} \geq 0. \tag{44}$$

We seek to enforce (44) for arbitrary values of arbitrary values for $\dot{\mathbf{F}}$, $\dot{\varphi}_{\mathrm{R}}^{\alpha}$, $\nabla\dot{\varphi}_{\mathrm{R}}^{\alpha}$, and $\nabla\mu_{\mathrm{R}}^{\alpha}$ at any instant and position.

Following the notation and the definition for the Larché–Cahn derivatives for both scalar and gradient fields as proposed by [23], the relative chemical potential $\mu_{\mathrm{R}\sigma}^{\alpha}$ results from the Larché–Cahn derivative as a consequence of incorporating the mass constraint given by (19). According to Larché–Cahn [15], the relative chemical potential expresses the chemical potential of α-th species measured relative to the chemical potential of σ-th species. This definition entails that, for saturated systems, the mass constraint given by (19) must always hold. Analogously, the relative microforce $\boldsymbol{\xi}_{\mathrm{R}\sigma}^{\alpha}$ emerges from the constraint imposed in the concentration gradients by (20). As a consequence, we rewrite (44) in the Larché–Cahn sense the following terms: $\pi^{\alpha} := \pi_{\sigma}^{\alpha}$, $\mu^{\alpha} := \mu_{\mathrm{R}\sigma}^{\alpha}$ and $\boldsymbol{\xi}_{\mathrm{R}}^{\alpha} := \boldsymbol{\xi}_{\mathrm{R}\sigma}^{\alpha}$ as well as the material mass fluxes $\boldsymbol{J}_{\mathrm{R}}^{\alpha} := \boldsymbol{J}_{\mathrm{R}\sigma}^{\alpha}$ as all these quantities are expressed relative to the σ-th reference species. Thus, the free-energy inequality is

$$\left(\mathbf{T}_{\mathrm{R}} - \frac{\partial\hat{\psi}}{\partial\mathbf{F}}\right) : \dot{\mathbf{F}} + \sum_{\alpha=1}^{n}\left(\mu_{\mathrm{R}\sigma}^{\alpha} - \pi_{\sigma}^{\alpha} - \frac{\partial^{(\sigma)}\hat{\psi}}{\partial\varphi_{\mathrm{R}}^{\alpha}}\right)\dot{\varphi}_{\mathrm{R}}^{\alpha} + \sum_{\alpha=1}^{n}\left(\boldsymbol{\xi}_{\mathrm{R}\sigma}^{\alpha} - \frac{\partial^{(\sigma)}\hat{\psi}}{\partial\nabla\varphi_{\mathrm{R}}^{\alpha}}\right)\cdot\nabla\dot{\varphi}_{\mathrm{R}}^{\alpha} - \sum_{\alpha=1}^{n}\left\{\boldsymbol{J}_{\mathrm{R}\sigma}^{\alpha}\cdot\nabla\mu_{\mathrm{R}\sigma}^{\alpha} + \mu_{\mathrm{R}\sigma}^{\alpha}s_{\mathrm{int}}^{\alpha}\right\} \geq 0. \tag{45}$$

The latter implies that the following relations must hold to keep consistency with the dissipation imbalance

$$\mathbf{T}_{\mathrm{R}} = \frac{\partial\hat{\psi}}{\partial\mathbf{F}}, \tag{46a}$$

$$\pi_{\sigma}^{\alpha} = \mu_{\mathrm{R}\sigma}^{\alpha} - \frac{\partial^{(\sigma)}\hat{\psi}}{\partial\varphi_{\mathrm{R}}^{\alpha}}, \tag{46b}$$

$$\boldsymbol{\xi}_{\mathrm{R}\sigma}^{\alpha} = \frac{\partial^{(\sigma)}\hat{\psi}}{\partial\nabla\varphi_{\mathrm{R}}^{\alpha}}. \tag{46c}$$

We use a logarithmic multi-well potential together with a multi-gradient-type potential for the chemical energy, that is,

$$\hat{\psi}^{ch}(\boldsymbol{\varphi}_{\mathrm{R}}, \nabla\boldsymbol{\varphi}_{\mathrm{R}}) = N_v k_B \vartheta \left(\sum_{\alpha=1}^{n} \varphi_{\mathrm{R}}^{\alpha} \ln \varphi_{\mathrm{R}}^{\alpha} \right) + N_v \sum_{\alpha=1}^{n} \sum_{\beta=1}^{n} \Omega^{\alpha\beta} \varphi_{\mathrm{R}}^{\alpha} \varphi_{\mathrm{R}}^{\beta} + \frac{1}{2} \sum_{\alpha=1}^{n} \sum_{\beta=1}^{n} \Gamma^{\alpha\beta} \nabla\varphi_{\mathrm{R}}^{\alpha} \cdot \nabla\varphi_{\mathrm{R}}^{\beta}. \tag{47}$$

This expression corresponds to the extension of the Cahn–Hilliard equation towards multicomponent systems [25,26]. The Ginzburg–Landau free energy governs the dynamics of the phase separation process undergoing spinodal decomposition. In (47), N_v is the number of molecules per unit volume, k_B is the Boltzmann constant, and $\Omega^{\alpha\beta}$ represents the interaction energy between the mass fraction of the α-th and β-th species. The interaction between the species α over β is reciprocal, thus $\Omega^{\alpha\beta}$ is symmetric. The interaction energy is positive and is related to the critical temperature for each pair of species, $\vartheta_c^{\alpha\beta}$, (between the α-th and β-th species). Following standard convention, we adopt that $\Omega^{\alpha\beta} = 0$ when $\alpha = \beta$ and $\Omega = 2k_B\vartheta_c^{\alpha\beta}$ when $\alpha \neq \beta$ [25–27]. Furthermore, $\Gamma^{\alpha\beta} = \sigma^{\alpha\beta}\ell^{\alpha\beta}$ [force] (no summation implied by the repeated indexes) represents the magnitude of the interfacial energy between the α-th and β-th species. The parameters $\sigma^{\alpha\beta}$ and $l^{\alpha\beta}$ are the interfacial tension [force/length] and the interfacial thickness [2] for each pair of species (between the α-th and β-th species) [length], respectively. In [25], the authors define the force $\Gamma^{\alpha\beta}$ as $N_v\Omega^{\alpha\beta}(\ell^{\alpha\beta})^2$.

Following [11], we assume that the elastic solid behaves as a compressible neo-Hookean material whose elastic energy is given by

$$\hat{\psi}^{el}(\mathbf{F}^e) = \frac{G}{2}\left[\mathbf{F}^e : \mathbf{F}^e - 3\right] + \frac{G}{\beta}\left[(\det\mathbf{F}^e)^{-\beta} - 1\right], \tag{48}$$

where G and β are material parameters that relate to the shear modulus and the weak compressibility of the material. β is a function of the Poisson ratio ν such that $\beta = 2\nu/1 - 2\nu$. In line with treatments of thermoelasticity, we assume a multiplicative decomposition of the deformation gradient [11], that is,

$$\mathbf{F}^e = \mathbf{F}^{\varphi}\mathbf{F}, \tag{49a}$$

$$\mathbf{F}^{\varphi} = \left(1 + \sum_{\alpha=1}^{n} \omega^{\alpha}(\varphi_{\mathrm{R}}^{\alpha} - \varphi_{\mathrm{R}0}^{\alpha})\right)^{-\frac{1}{3}} \mathbf{I}, \tag{49b}$$

$$\mathbf{F}^{\varphi} = \mathrm{J}_{\varphi}^{-\frac{1}{3}}\mathbf{I}. \tag{49c}$$

This expression suggests that when the local species concentrations change relative to their initial distribution, the solid must undergo elastic deformation. The swelling material parameter ω^{α} is associated with the molar volume of the solute, the volume occupied by a mol of each species scaled by the maximum concentration [10,11]. More recent works suggest that ω^{α} can be modelled as a dilation tensor or as a function of the overall reaction rate [28,29].

The evolution of the conserved field $\varphi_{\mathrm{R}}^{\alpha}$ obeys a non-Fickian diffusion driven by the chemical potential differences between the species. We combine (46b) and (46c) using the balance of microforces (30) and the constitutive relation for the free energy (41) to express the relative chemical potential of the α-th species as

$$\mu_{\mathrm{R}\sigma}^{\alpha} = \frac{\partial^{(\sigma)}\hat{\psi}}{\partial\varphi_{\mathrm{R}}^{\alpha}} - \mathrm{Div}\frac{\partial^{(\sigma)}\hat{\psi}}{\partial\nabla\varphi_{\mathrm{R}}^{\alpha}} - (\gamma^{\alpha} + \gamma^{\sigma}), \tag{50}$$

and therefore,

$$\begin{aligned}\mu_{\mathrm{R}\sigma}^{\alpha} = {} & N_v k_B \vartheta \left(\ln\frac{\varphi_{\mathrm{R}}^{\alpha}}{\varphi_{\mathrm{R}}^{\sigma}}\right) + 2N_v \sum_{\beta=1}^{n} (\Omega^{\alpha\beta} - \Omega^{\sigma\beta})\varphi_{\mathrm{R}}^{\beta} \\ & - \sum_{\beta=1}^{N} (\Gamma^{\alpha\beta} - \Gamma^{\sigma\beta})\,\mathrm{Div}\nabla\varphi_{\mathrm{R}}^{\beta} - \frac{1}{3}\omega_{\sigma}^{\alpha}\mathrm{J}_{\varphi}^{-1}\mathrm{tr}[\mathbf{T}_{\mathrm{R}}\mathbf{F}^{\top}] - (\gamma^{\alpha} + \gamma^{\sigma}),\end{aligned} \tag{51}$$

[2] This expression corresponds to the root mean square of the effective "interaction distance", as suggested by the work of Cahn and Hilliard [25].

Table 1 Coupled system of chemo-mechanical partial differential equations

Fundamental balances and constitutive responses	Equation
Balance solid mass	$\rho_0 = J\rho$
Balance species concentration	$\dot{\varphi}^{\alpha}_{\mathrm{R}} = s^{\alpha} - \mathrm{Div}\, \boldsymbol{J}^{\alpha}_{\mathrm{R}\sigma}$
Species mass flux	$\boldsymbol{J}^{\alpha}_{\mathrm{R}\sigma} = -\sum_{\beta=1}^{n} \boldsymbol{M}^{\alpha\beta}\, J\mathbf{C}^{-1}\nabla\mu^{\beta}_{\mathrm{R}\sigma}$
Species chemical potential	$\mu^{\alpha}_{\mathrm{R}\sigma} = \frac{\partial^{(\sigma)}\psi}{\partial\varphi^{\alpha}_{\mathrm{R}}} - \mathrm{Div}\,\frac{\partial^{(\sigma)}\psi}{\partial(\nabla\varphi^{\alpha}_{\mathrm{R}})} - (\gamma^{\alpha} + \gamma^{\sigma})$
Chemical reaction source term	$s^{\alpha}_{\mathrm{int}} = -\sum_{c=1}^{N_s}(\upsilon_{\alpha c} - \varpi_{\alpha c})(k^{+}_{c}\prod_{a=1}^{n}(\varphi^{a}_{\mathrm{R}})^{\upsilon_{ac}} - k^{-}_{c}\prod_{a=1}^{n}(\varphi^{a}_{\mathrm{R}})^{\varpi_{ac}})$
Balance linear momentum	$\mathbf{0} = \mathrm{Div}\,\mathbf{T}_{\mathrm{R}} + \mathbf{b}$
Stress tensor	$\mathbf{T}_{\mathrm{R}} = G\mathrm{J}_{\varphi}^{-1/3}[\mathbf{F}^{e} - (\det\mathbf{F}^{e})^{-\beta}\mathbf{F}^{e-\top}]$

where

$$\omega^{\alpha}_{\sigma} = \omega^{\alpha} - \omega^{\sigma}. \tag{52}$$

The constitutive relation for the first Piola-Kirchhoff stress tensor is

$$\mathbf{T}_{\mathrm{R}} = G\mathrm{J}_{\varphi}^{-1/3}[\mathbf{F}^{e} - (\det\mathbf{F}^{e})^{-\beta}\mathbf{F}^{e-\top}]. \tag{53}$$

We also consider the off-diagonal terms in the Onsager reciprocal relations and thus, we describe the species fluxes as

$$\boldsymbol{J}^{\alpha}_{\mathrm{R}\sigma} \overset{\mathrm{def}}{=} -\sum_{\beta=1}^{n} \boldsymbol{M}^{\alpha\beta}\, J\mathbf{C}^{-1}\nabla\mu^{\beta}_{\mathrm{R}\sigma}, \tag{54}$$

where $\boldsymbol{M}^{\alpha\beta}$ are the Onsager mobility coefficients. We use the standard assumption that the mobility coefficients depend on the phase composition. In particular, we express this dependency in terms of the concentration of each species. We use the definition $\boldsymbol{M}^{\alpha\beta} = M^{\alpha\beta}\varphi^{\alpha}_{\mathrm{R}}(\delta^{\alpha\beta} - \varphi^{\beta}_{\mathrm{R}})\mathbf{I}$ (no summation implied by the repeated indexes) where $\delta^{\alpha\beta}$ and $M^{\alpha\beta}$ are the Kronecker delta of dimension n and the mobility coefficients [26], respectively.

3 Dimensionless forms of the chemo-mechanical equations

This section presents the main equations and variables for the thermodynamically consistent theory for mineral solid solutions following Sect. 2. Table 1 summarises fundamental balance equations together with constitutive chemo-mechanical responses.

Moreover, we introduce a free-energy density $\psi_0 = 2N_v k_B\vartheta$ together with a set of diffusion coefficients $\boldsymbol{D}^{\alpha\beta}$ such that

$$\boldsymbol{D}^{\alpha\beta} = \psi_0\boldsymbol{M}^{\alpha\beta} \tag{55}$$

To make the governing and constitutive equations dimensionless (Table 1), we define the following dimensionless variables

$$\overline{\mathbf{u}} = u_0^{-1}\mathbf{u}, \qquad \overline{\mathbf{x}} = L_0^{-1}\mathbf{x}, \qquad \overline{t} = D_0 l_0^2 L_0^{-4} t \tag{56}$$

where u_0, D_0, and l_0 account for a reference deformation state, the diffusion coefficient, and the interface thickness of a reference species, respectively. We propose the following sets of scalar and vector dimensionless numbers for the multicomponent chemo-mechanical system, that is,

$$\begin{aligned}
&\omega^{\alpha},\ \overline{k}^{c}_{+} = k^{c}_{+}D_0^{-1}\ell_0^{-2}L_0^{4},\ \overline{k}^{c}_{-} = k^{c}_{-}D_0^{-1}\ell_0^{-2}L_0^{4},\ \overline{\vartheta}^{\alpha\beta}_{c} = \vartheta^{-1}\vartheta^{\alpha\beta}_{c},\\
&\overline{\ell}^{\alpha\beta} = L_0^{-1}\ell^{\alpha\beta},\ \overline{\psi} = \hat{\psi}\psi_0^{-1},\ \overline{\sigma}^{\alpha\beta} = \sigma^{\alpha\beta}(\psi_0 L_0)^{-1},\ \beta,\ \overline{\mathbf{b}} = G^{-1}\mathbf{b},\\
&\overline{G} = G\psi_0^{-1},\ l = u_0 L_0^{-1},\ \overline{\boldsymbol{D}}^{\alpha\beta} = \boldsymbol{D}^{\alpha\beta}D_0^{-1}\ell_0^{-2}L_0^{2},\ \overline{\gamma}^{\alpha} = \psi_0^{-1}\gamma^{\alpha}.
\end{aligned} \tag{57}$$

By inserting the dimensionless quantities in (47) and (48), we find the following dimensionless forms of the chemical energy

$$\overline{\psi}^{ch}(\boldsymbol{\varphi}_{\mathrm{R}}, \overline{\nabla}\boldsymbol{\varphi}_{\mathrm{R}}) = \frac{1}{2}\left(\sum_{\alpha=1}^{n} \varphi_{\mathrm{R}}^{\alpha} \ln \varphi_{\mathrm{R}}^{\alpha}\right) + \sum_{\alpha=1}^{n}\sum_{\beta=1}^{n} \overline{\vartheta}_{c}^{\alpha\beta} \varphi_{\mathrm{R}}^{\alpha}\varphi_{\mathrm{R}}^{\beta} + \frac{1}{2}\sum_{\alpha=1}^{n}\sum_{\beta=1}^{n} \overline{\sigma}^{\alpha\beta}\overline{\ell}^{\alpha\beta}\, \overline{\nabla}\varphi_{\mathrm{R}}^{\alpha} \cdot \overline{\nabla}\varphi_{\mathrm{R}}^{\beta}, \tag{58}$$

and the mechanical energy

$$\overline{\psi}^{el}(\overline{\mathbf{F}^{e}}) = \overline{G}\left\{\frac{1}{2}\left[\overline{\mathbf{F}^{e}} : \overline{\mathbf{F}^{e}} - 3\right] + \frac{1}{\beta}\left[(\det\overline{\mathbf{F}^{e}})^{-\beta} - 1\right]\right\}, \tag{59}$$

where $\overline{\mathbf{F}^{e}} = \mathrm{J}_{\varphi}^{-1/3}(\mathbf{I} + l\overline{\nabla}\overline{\mathbf{u}})$. We also define the dimensionless bulk free energy as

$$\overline{\psi}^{\varphi}(\boldsymbol{\varphi}_{\mathrm{R}}) = \frac{1}{2}\left(\sum_{\alpha=1}^{n} \varphi_{\mathrm{R}}^{\alpha} \ln \varphi_{\mathrm{R}}^{\alpha}\right) + \sum_{\alpha=1}^{n}\sum_{\beta=1}^{n} \overline{\vartheta}_{c}^{\alpha\beta} \varphi_{\mathrm{R}}^{\alpha}\varphi_{\mathrm{R}}^{\beta} \tag{60}$$

Likewise, the dimensionless forms of the governing and constitutive equations read

$$\begin{aligned}
\frac{\partial \varphi_{\mathrm{R}}^{\alpha}}{\partial \bar{t}} &= \overline{\nabla} \cdot \left(\sum_{\beta=1}^{n} \overline{\boldsymbol{D}}^{\alpha\beta}\overline{\boldsymbol{M}}\, \overline{\nabla}\overline{\mu}_{\mathrm{R}\sigma}^{\beta}\right) + \overline{s}^{\alpha},\\
\overline{\boldsymbol{M}} &= \det(\mathbf{I} + l\overline{\nabla}\overline{\mathbf{u}})(\mathbf{I} + l\overline{\nabla}\overline{\mathbf{u}})^{-1}(\mathbf{I} + l\overline{\nabla}\overline{\mathbf{u}})^{-\top},\\
\overline{\mu}_{\mathrm{R}\sigma}^{\alpha} &= \frac{1}{2}\left(\ln\frac{\varphi_{\mathrm{R}}^{\alpha}}{\varphi_{\mathrm{R}}^{\sigma}}\right) + 2\sum_{\beta=1}^{n}(\overline{\vartheta}_{c}^{\alpha\beta} - \overline{\vartheta}_{c}^{\alpha\beta})\varphi_{\mathrm{R}}^{\beta} - \sum_{\beta=1}^{N}(\overline{\sigma}^{\alpha\beta}\overline{\ell}^{\alpha\beta} - \overline{\sigma}^{\sigma\beta}\overline{\ell}^{\sigma\beta})\,\overline{\Delta}\varphi_{\mathrm{R}}^{\beta}\\
&\quad - \frac{1}{3}\omega^{\alpha\sigma}\mathrm{J}_{\varphi}^{-1}\overline{G}\,\mathrm{tr}[\overline{\mathbf{T}}_{\mathrm{R}}(\mathbf{I} + l\overline{\nabla}\overline{\mathbf{u}})^{\top}] - (\overline{\gamma}^{\alpha} + \overline{\gamma}^{\sigma}),\\
\overline{s}_{\mathrm{int}}^{\alpha} &= -\sum_{c=1}^{n_s}\left\{(\upsilon^{c\alpha} - \varpi^{c\alpha})(\overline{k}_{+}^{c}\prod_{a=1}^{n}(\varphi_{\mathrm{R}}^{a})^{\upsilon^{ca}} - \overline{k}_{-}^{c}\prod_{a=1}^{n}(\varphi_{\mathrm{R}}^{a})^{\varpi^{ca}})\right\},\\
\mathbf{0} &= \mathrm{Div}\,\overline{\mathbf{T}}_{\mathrm{R}} + \overline{\mathbf{b}},\\
\overline{\mathbf{T}}_{\mathrm{R}} &= \mathrm{J}_{\varphi}^{-1/3}[\mathrm{J}_{\varphi}^{-\frac{1}{3}}(\mathbf{I} + l\overline{\nabla}\overline{\mathbf{u}}) - (\det\mathrm{J}_{\varphi}^{-\frac{1}{3}}(\mathbf{I} + l\overline{\nabla}\overline{\mathbf{u}})^{-\beta}(\mathrm{J}_{\varphi}^{-\frac{1}{3}}(\mathbf{I} + l\overline{\nabla}\overline{\mathbf{u}}))^{-\top}],
\end{aligned} \tag{61}$$

Hence, the set of equations (61) encompasses a system of partial differential equations, that subject to both initial and boundary conditions, allows us to evolve the governing variables in this closed system: species concentrations $\varphi_{\mathrm{R}}^{\alpha}$, chemical potentials $\overline{\mu}_{\mathrm{R}\sigma}^{\alpha}$, and solid displacements $\overline{\mathbf{u}}$.

4 Numerical simulations of 2D and 3D ternary systems

In this section, we present 2D and 3D simulations of the temporal evolution of single materials modelled as a solid solution composed of three phases $\mathcal{A}^1$, $\mathcal{A}^2$, and $\mathcal{A}^3$ to investigate their coupled chemo-mechanical interactions. In particular, the 2D simulation shows how interfacial interactions, together with a reversible chemical reaction between the phases, engender volumetric stresses as a result of local volume changes. While the 3D simulation studies a ripening mechanism. The interfacial interactions between the phases drive the phase separation process and allow for the Ostwald ripening and Gibbs-Thomson effects. We show the dimensionless temporal evolution of the dimensionless phases concentrations as well as the dimensionless displacements in each coordinate direction. By doing so, we seek to understand the interleaving between the physical and the chemical responses of the mineral solid solutions. Figure 1 plots the bulk energy surface for the ternary multi-well potential of (60) for a ternary system.

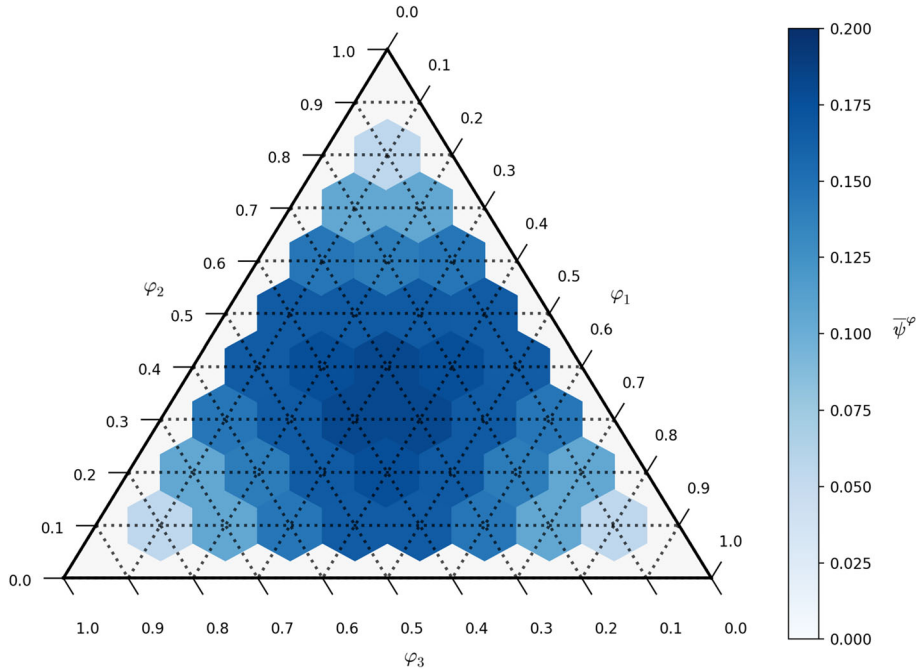

Fig. 1 Dimensionless bulk energy surface plot for the ternary multi-well potential

4.1 Reversible chemical reaction of random distributed phases

The reversible chemical reaction between the phases is

$$\mathcal{A}^1 + \mathcal{A}^2 \underset{k_-}{\overset{k_+}{\rightleftharpoons}} 2\mathcal{A}^3, \tag{62}$$

where the stoichiometry vectors $\upsilon^{\alpha\beta}$ and $\varpi^{\alpha\beta}$ are given by

$$\upsilon^{\alpha\beta} = (1, 1, 0), \qquad \text{and} \qquad \varpi^{\alpha\beta} = (0, 0, 2). \tag{63}$$

We study the stress-assisted volume changes triggered by the chemical processes. Therefore, we do not drive the deformation by distorting the analysis domain. We set the external body forces and external microforces such that $\mathbf{b} = \mathbf{0}$ and $\gamma^{\alpha} = 0$, respectively. Moreover, we neglect all inertial effects. Consequently, the spatial velocity $\boldsymbol{v}$ is nearly constant through the time. We assume that the three phases diffuse at the same rate. Therefore, we only consider one diffusion coefficient. In this simulation example, we set $k_+ > k_-$. Thus, the forward chemical reaction occurs faster than the backward one. Our initial condition serves as the reference configuration, which we choose as an undeformed state of the body. The mass supply of each phase, captured by the reaction term s^{α}, results solely from internal contributions as the system (62) reacts. The initial spatial distribution of the phase concentrations is random such that φ^{α} takes values between $\varphi^{\alpha} \pm 0.05$ where we assume φ^{α} is $1/n$. We calculate the concentration of $\mathcal{A}^3$ following the mass constraint given by (19). As mentioned before, we apply this mass constraint when we compute the relative quantities resulting from the Larché–Cahn derivative. By doing so, we guarantee the consistency of the process. Furthermore, there is no mass flux at the solid boundaries.

Figure 2a shows the spatial distribution of the initial phases concentrations in conjunction with the initial displacements. We set the parameters in the chemical energy such that we obtain a triple-well function. This function allows us to model the phase separation process. The reactive system seeks to minimize its global free energy. Thus, the reaction drives the given initial concentrations for the phases $\mathcal{A}^1$, $\mathcal{A}^2$, and $\mathcal{A}^3$ towards the concentrations at the well points.

Table 2 summarises the parameters used to build up the dimensionless numbers (64) as outlined in (57).

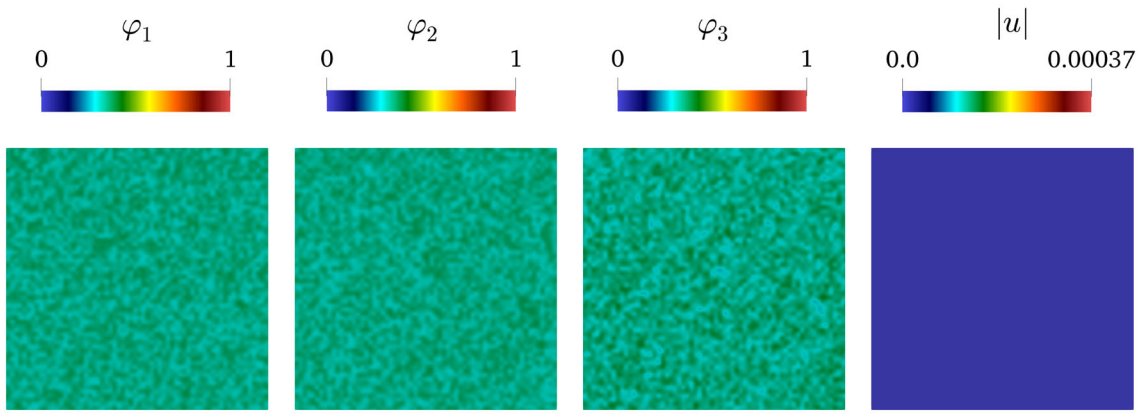

(a) $\bar{t} = 0$

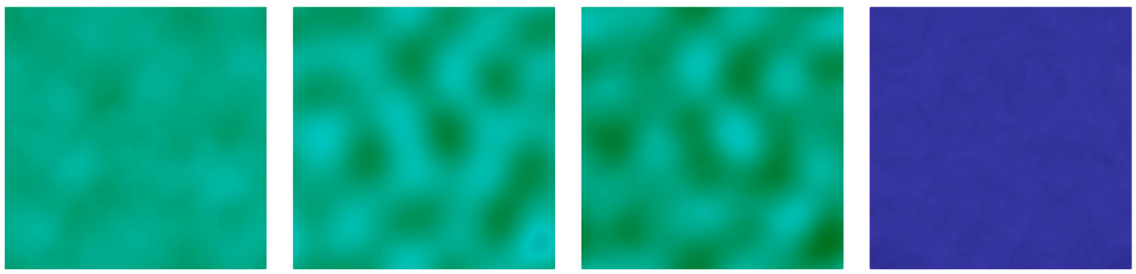

(b) $\bar{t} = 4.04 \times 10^{-6}$

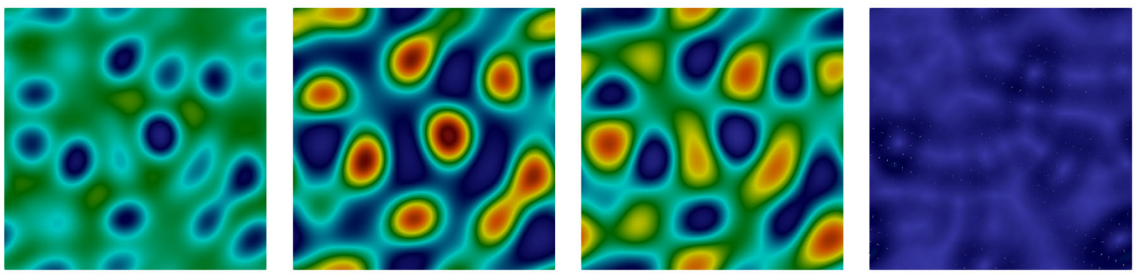

(c) $\bar{t} = 9.03 \times 10^{-6}$

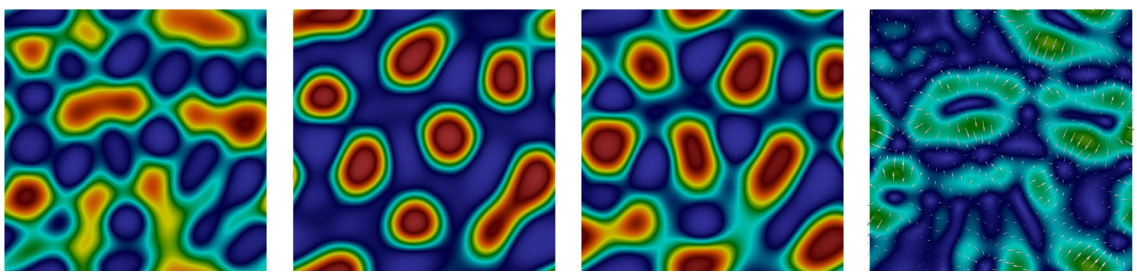

(d) $\bar{t} = 1.26 \times 10^{-5}$

Fig. 2 Temporal evolution of the three phase fields together with the magnitude of the displacement vector and its direction at early stages

Table 2 Chemical and physical parameters that control the spinodal decomposition process

Physical parameter	Value	Name
ψ_0 [J m^{-3}]	1×10^5	Energy density
L_0 [m]	10^{-6}	Domain length
u_0 [m]	10^{-6}	Reference displacement
G [GPa]	40	Shear modulus
β [-]	0.17	Poisson's ratio
ϑ [K]	727.0	Absolute temperature
ϑ_c^{12} [K]	800.0	Critical temperature between phases 1 and 2
ϑ_c^{13} [K]	800.0	Critical temperature between phases 1 and 3
ϑ_c^{23} [K]	800.0	Critical temperature between phases 2 and 3
D [m^{2}s^{-1}]	10^{-20}	Diffusion coefficient (same for all phases)
k_+ [m^{2}s^{-1}]	10^{-14}	Forward reaction rate
k_- [m^{2}s^{-1}]	10^{-16}	Backward reaction rate
σ [J m^{-2}]	0.817	Interfacial energy
ℓ [m]	10^{-8}	Interface thickness
γ [-]	0	External microforce (same for all phases)
$\mathbf{b}$ [ms^{-2}]	$\mathbf{0}$	Body force

Hence, the diffusion matrix for each entry α and β as well as the dimensionless numbers are given by

$$\begin{gathered}\bar{\boldsymbol{D}}^{\alpha\beta} = 1 \times 10^4 \varphi^\alpha(\delta^{\alpha\beta} - \varphi^\beta)\mathbf{I} \quad \forall\, 1 \le \alpha, \beta \le n, \quad \bar{\vartheta}_c^{\alpha\beta} = \begin{bmatrix} 0 & 1.100 & 1.100 \\ 1.100 & 0 & 1.100 \\ 1.100 & 1.100 & 0 \end{bmatrix}, \\ \bar{\sigma}^{\alpha\beta}\bar{\ell}^{\alpha\beta} = 10^{-2}\begin{bmatrix} 8.17 & 0 & 0 \\ 0 & 8.17 & 0 \\ 0 & 0 & 8.17 \end{bmatrix}, \quad \upsilon^{\alpha\beta} = \begin{bmatrix} 1\ 1\ 0 \end{bmatrix}, \\ \varpi^{\alpha\beta} = \begin{bmatrix} 0\ 0\ 2 \end{bmatrix}, \quad \bar{k}_+ = 0.01, \quad \bar{k}_- = 0.0001, \quad \overline{G} = 4 \times 10^5 \\ \omega^1 = 0.0383 \quad \omega^2 = 0.0334 \quad \omega^3 = 0.0165 \end{gathered} \tag{64}$$

where we choose $D_0 = D$ and $\ell_0 = \ell$ as the reference diffusion coefficient and interface thickness of a reference phase, respectively, where swelling parameter is dimensionless in nature as it is scaled by the maximum concentration.

The final system of coupled chemo-mechanical equations is

$$\dot{\varphi}^1 = -k_+\varphi^1\varphi^2 + k_-(\varphi^3)^2 - \operatorname{Div} \boldsymbol{J}^1_{\mathrm{R}3}, \tag{65a}$$

$$\dot{\varphi}^2 = -k_+\varphi^1\varphi^2 + k_-(\varphi^3)^2 - \operatorname{Div} \boldsymbol{J}^2_{\mathrm{R}3}, \tag{65b}$$

$$\operatorname{Div} \mathbf{T}_{\mathrm{R}} = \mathbf{0}. \tag{65c}$$

In (65), we use the Larché–Cahn derivative with $\mathcal{A}^3$ as the reference phase. We solve the system of partial differential equations in its primal form (66) and (68). We state the problem as follows: find $\{\varphi, \mathbf{u}\} \in \mathcal{C}^2(\mathbf{P})$ such that (61) subjected to periodic boundary conditions up to the second derivative of φ, and $\mathbf{u}$ with respect to $\mathbf{X}$ in a square open region $\mathbf{B} = (0, 1) \times (0, 1)$. We use PetIGA [30], a high-performance isogeometric analysis framework built on top of PETSc [31]. We use a mesh with 64×64 elements of a polynomial degree 2 and continuity 1.

We denote H^2 as the Sobolev space of square integrable functions with square integrable first and second derivatives and $(\cdot, \cdot)_{\mathbf{P}}$ as the L^2 inner product over an arbitrary material part $\mathbf{P}$ with boundary S. We multiply the Lagrangian version of the phases mass balance (16) by a test function ϱ^α, which belongs to H^2, using the definition for the material mass fluxes (54) and integrating by parts, the primal variational formulation is

$$
\begin{aligned}
(\varrho^\alpha, \dot{\varphi^\alpha})_{\mathbf{P}} &= (\varrho^\alpha, s^\alpha)_{\mathbf{P}} - (\varrho^\alpha, J^\alpha_{\mathrm{R}\sigma I,I})_{\mathbf{P}} \\
&= (\varrho^\alpha, s^\alpha)_{\mathbf{P}} + (\varrho^\alpha_{,I}, J^\alpha_{\mathrm{R}\sigma I})_{\mathbf{P}} - (\varrho^\alpha, J^\alpha_{\mathrm{R}\sigma I} N_I)_{\mathrm{S}} \\
&= (\varrho^\alpha, s^\alpha)_{\mathbf{P}} + (\varrho^\alpha_{,I}, -M^{\alpha\beta}(\mu^\beta_\varphi + \mu^\beta_s + p^\beta_\varphi)_{,J} C^{-1}_{JI} J)_{\mathbf{P}} \\
&\quad - (\varrho^\alpha, -M^{\alpha\beta}(\mu^\beta_{,J}) C^{-1}_{JI} J N_I)_{\mathrm{S}} \\
&= (\varrho^\alpha, s^\alpha)_{\mathbf{P}} - (\varrho^\alpha_{,I}, M^{\alpha\beta}\mu^\beta_{\varphi,J} C^{-1}_{JI} J)_{\mathbf{P}} - (\varrho^\alpha_{,I}, (M^{\alpha\beta}\mu^\beta_s)_{,J} C^{-1}_{JI} J)_{\mathbf{P}} \\
&\quad + (\varrho^\alpha_{,I}, (M^{\alpha\beta}_{,J})\mu^\beta_s C^{-1}_{JI} J)_{\mathbf{P}} - (\varrho^\alpha_{,I}, M^{\alpha\beta} p^\beta_{\varphi,J} C^{-1}_{JI} J)_{\mathbf{P}} \\
&\quad + (\varrho^\alpha, M^{\alpha\beta}(\mu^\beta_{,J}) C^{-1}_{JI} J N_I)_{\mathrm{S}} \\
&= (\varrho^\alpha, s^\alpha)_{\mathbf{P}} - (\varrho^\alpha_{,I}, M^{\alpha\beta}\mu^\beta_{\varphi,J} C^{-1}_{JI} J)_{\mathbf{P}} + (\varrho^\alpha_{,IJ} C^{-1}_{JI} J, M^{\alpha\beta}\mu^\beta_s)_{\mathbf{P}} \\
&\quad + (\varrho^\alpha_{,I}(C^{-1}_{JI} J)_{,J}, M^{\alpha\beta}\mu^\beta_s)_{\mathbf{P}} + (\varrho^\alpha_{,I}, (M^{\alpha\beta}_{,J})\mu^\beta_s C^{-1}_{JI} J)_{\mathbf{P}} \\
&\quad - (\varrho^\alpha_{,I}, M^{\alpha\beta} p^\beta_{\varphi,J} C^{-1}_{JI} J)_{\mathbf{P}} + (\varrho^\alpha, M^{\alpha\beta}(\mu^\beta_{,J}) N_I C^{-1}_{JI} J)_{\mathrm{S}}. \\
&\quad - (\varrho^\alpha_{,I} N_J C^{-1}_{JI} J, M^{\alpha\beta}\mu^\beta_s)_{\mathrm{S}}
\end{aligned} \tag{66}
$$

where for convenience, we split the chemical potential $\mu^\alpha_{\mathrm{R}\sigma}$ such that $\mu^\alpha_{\mathrm{R}\sigma} = \mu^\alpha_\varphi + \mu^\alpha_s + p^\alpha_\varphi$. Thereby,

$$
\begin{aligned}
\mu^\alpha_\varphi &= N_v k_B \vartheta \left(\ln \frac{\varphi^\alpha_{\mathrm{R}}}{\varphi^\sigma_{\mathrm{R}}} \right) + 2N_v \sum_{\beta=1}^{n} (\Omega^{\alpha\beta} - \Omega^{\sigma\beta})\varphi^\beta_{\mathrm{R}} - (\gamma^\alpha + \gamma^\sigma), \\
\mu^\alpha_s &= -\sum_{\beta=1}^{N} (\Gamma^{\alpha\beta} - \Gamma^{\sigma\beta}) \operatorname{Div} \nabla \varphi^\beta_{\mathrm{R}}, \\
p^\alpha_\varphi &= \omega^\alpha_\sigma \mathrm{J}^{-1}_\varphi p.
\end{aligned} \tag{67}
$$

We define $p := -\frac{1}{3}\mathrm{tr}[\mathbf{T}_{\mathrm{R}}\mathbf{F}^\top]$ as the mechanical pressure (which differs from the thermodynamic pressure) and emphasize that this pressure modifies the mass transport rate. Therefore, for deformable bodies undergoing mass transport, this physical quantity alters the driving force of the chemical process. Furthermore, the weak formulation of the Lagrangian version of the linear momenta balance reads

$$
(w_i, \mathrm{T}_{\mathrm{R}iI} N_I)_{\mathrm{S}} - (w_{i,I}, \mathrm{T}_{\mathrm{R}iI})_{\mathbf{P}} = 0, \tag{68}
$$

where we multiply (25) by a test function w_i.

At early stages Fig. 2b, $\bar{t} < 4.04 \times 10^{-6}$, the solution goes through an initial spinodal decomposition. This spontaneous phase separation process occurs due to $\vartheta_c^{\alpha\beta} > \vartheta$. Otherwise, the mixture would only diffuse without unmixing. As the phases $\mathcal{A}^i$, $i = 1, 2, 3$, diffuse as a result of their separation, the solid undergoes elastic deformation due to the mass transport. Analogously, the pressure p^α_φ alters the rate at which the phases diffuse. The deformation arises solely from mass transport since the reversible chemical reaction has no significant impact. From Fig. 4, we verify that the phases masses do not change substantially in the range $0 < \bar{t} < 4.04 \times 10^{-6}$. As a consequence, there is no nucleation and growth of phases. With regards to the interfacial energies, in the range $0 < \bar{t} < 4.04 \times 10^{-6}$ the energies decrease gently up to a point, $\bar{t} \simeq 1.0 \times 10^{-7}$, where the interfacial energies become constant. A small change in the interfacial energies means that either the phase separation has not evolved significantly or there is no substantial coarsening. Furthermore, at the early stages, the deformation is small as the displacements (see Fig. 2) are not large since the phase separation has not evolved such that the phases are unmixed. As expected, the displacements u_x and u_y in the solid move following the mass transport.

Later on, in the range between $4.04 \times 10^{-6} < \bar{t} < 9.03 \times 10^{-6}$, the phase separation becomes prominent as it allows to form spatial domains rich in each component (see Fig. 2c). In particular, the phase $\mathcal{A}^1$ remains partially unmixed as there are no rounded inclusions with large concentration (see Fig. 2c). On the contrary, for phases $\mathcal{A}^2$ and $\mathcal{A}^3$, rounded inclusions with large concentrations appear. At this stage, there is no influence of the chemical reaction (see Fig. 4). Larger displacements are collocated with the larger inclusions for $\mathcal{A}^2$ and $\mathcal{A}^3$. This collocation is a consequence of the mass flux towards these points as the inclusions grow. The

enlargement associated with the growth of the inclusions induces deformation. $\mathbf{F}^{\varphi}$ captures this behavior. The interfacial energies remain roughly constant, which implies that there is a balance between both the creating and disassemble of phases interfaces. As expected, in the time interval between $0 < \bar{t} < 9.03 \times 10^{-6}$, the tendency of the global free energy is monotonically decreasing as the system goes to a steady state of maximum entropy (see Fig. 5). This free energy encompasses the contribution from both the chemical and the mechanical energies. At the early stages, as the evolution towards a steady-state goes on, the system favors phase separation.

For instance, Fig. 2d shows the evolution of small $\mathcal{A}^1$ inclusions in the range between $9.03 \times 10^{-6} < \bar{t} < 1.26 \times 10^{-5}$. As suggested before, there is mass flux towards these points that allows the inclusion to grow and deform the solid. Figure 2d also shows the larger displacements in the regions where the inclusions are. On the other hand, $\mathcal{A}^3$ inclusions are large and close enough to start merging. This phenomenon is associated with the minimization of the global free energy as the system reduces its interfacial energies. Nevertheless, when considering the system undergoing chemical reactions, the interfacial energies evolve according to the chemical reaction, which in this modeling example corresponds to a reversible chemical reaction. The growth of more $\mathcal{A}^3$ as a result of the reversible chemical reaction creates more $\mathcal{A}^3$ interface. Figure 4 shows an increase in $\mathcal{A}^3$ interfacial energy as well as its mass. On the other hand, the decomposition of $\mathcal{A}^3$ into $\mathcal{A}^1$ and $\mathcal{A}^2$ following (62) must increase $\mathcal{A}^1$ and $\mathcal{A}^2$ masses, and their interfacial energies. However, this behavior does not last since the rate of creation of $\mathcal{A}^3$ is faster than the decomposition into $\mathcal{A}^1$ and $\mathcal{A}^2$. This is due to $k_+ >> k_-$.

From $\bar{t} = 5.64 \times 10^{-5}$, the system shows the merging of large inclusions and the action of the reversible chemical reaction (see Fig. 3a). At this stage, the creation of $\mathcal{A}^3$ predominates. One can verify such an assertion by checking the masses. However, there is no interfacial energy growth since the larger inclusions are merging. Therefore, the interfacial energies decrease. Moreover, the $\mathcal{A}^1$, $\mathcal{A}^2$, and $\mathcal{A}^3$ inclusions pass from rounded to square-like structures. Such behavior results from the dependency of the chemical potential upon the pressure p_{φ}^{α} caused by deformation and the Gibbs-Thomson effect associated with the curvature $\Delta\varphi_{\mathrm{R}}^{\alpha}$. Along the boundaries of the inclusions, the driving force of the mass transport changes, which may generate inclusions of asymmetric morphologies. Moreover, the creation of $\mathcal{A}^1$, $\mathcal{A}^2$, and $\mathcal{A}^3$ following (62) engenders a mechanical pressure associated with nucleation and growth. Figure 3a also shows the large displacements at the phase boundaries that account for the impact of the chemical reaction on the stress generation (pressure).

Figure 3b shows the state at $\bar{t} = 4.26 \times 10^{-4}$. The system forms a chain-like structure composed of the phases $\mathcal{A}^1$ and $\mathcal{A}^2$, which is surrounded by the phase $\mathcal{A}^3$. This structure emerges as a result of the merging processes and the reversible chemical reaction. The reversible chemical reaction continues to take at the boundary between phases $\mathcal{A}^1$ and $\mathcal{A}^2$. Moreover, the phase $\mathcal{A}^3$ decomposes into $\mathcal{A}^1$ and $\mathcal{A}^2$. At this point in the evolution, the phase $\mathcal{A}^3$ composes almost the whole solid due to $k_+ >> k_-$. The masses and interfacial energies for phases $\mathcal{A}^1$ and $\mathcal{A}^2$ decrease (see Fig. 4). However, for phase $\mathcal{A}^3$, the mass increases while reducing its interfacial energy (see Fig. 4). The phases are unmixed, whereby their concentrations correspond to the concentrations at the well points in the triple-well function. The displacements u_x and u_y are in the range of the previous stages. However, they move as the phases diffuse as a result of the relation between mass transport and deformation. Figure 3b depicts the larger displacements are in line with the chain-like structure.

Figure 3c shows the evolution at $\bar{t} = 5.72 \times 10^{-4}$. The minimization of the global free energy as the system goes to the steady-state reduces the thickness of the chain-like structure. Eventually, the chain is composed of interleaved inclusions of phases $\mathcal{A}^1$ and $\mathcal{A}^2$. As the inclusions of $\mathcal{A}^1$ and $\mathcal{A}^2$ become smaller, the phase $\mathcal{A}^3$ encloses $\mathcal{A}^1$ and $\mathcal{A}^2$. The interfacial energies and masses keep decreasing since the action of the reversible chemical reaction has not ceased (see Fig. 4). The displacement field shows the interaction between the mechanical and chemical processes. We observe smaller displacements inside the chain-like structure and larger ones outside this region.

In the time interval between $5.72 \times 10^{-4} < \bar{t} < 1.84 \times 10^{-3}$, the inclusions of phases $\mathcal{A}^1$ and $\mathcal{A}^2$ shrink as the reversible reaction continues (see Fig. 3d). When the reversible chemical reaction ceases, the inclusions are rounded. The chemical reaction is active between $1 \times 10^{-5} < t < \times 10^{-2}$. The larger (smaller) displacements appear around the inclusions of phase $\mathcal{A}^1$ ($\mathcal{A}^2$). These phases partially consume while the phase $\mathcal{A}^3$ gains mass. Finally, rounded structures composed of the three phases diffuse in the solid to generate displacements associated with mass transport. Figure 3e portrays such a behaviour. Along with the whole evolution, free energy always behaves monotonically decreasing (see Fig. 5). Figure 6 shows the microstructural configuration at the steady-state.

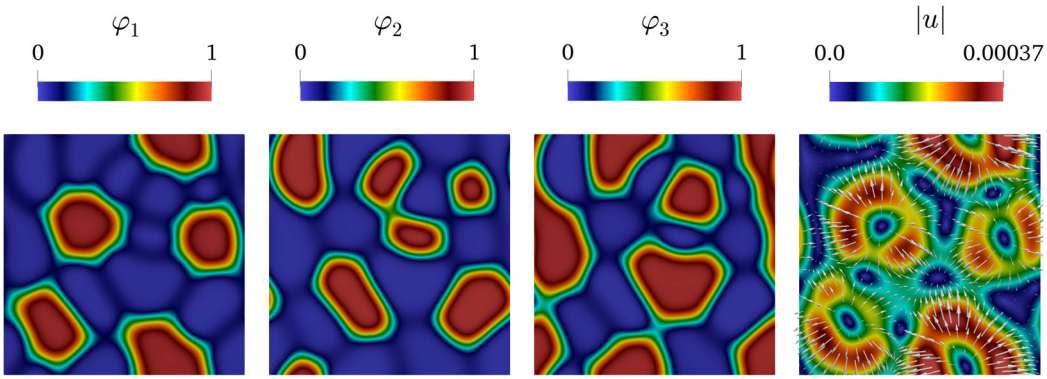

(a) $\bar{t} = 5.64 \times 10^{-5}$

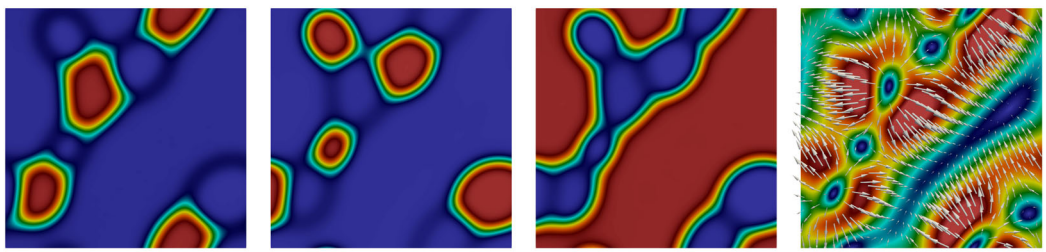

(b) $\bar{t} = 4.26 \times 10^{-4}$

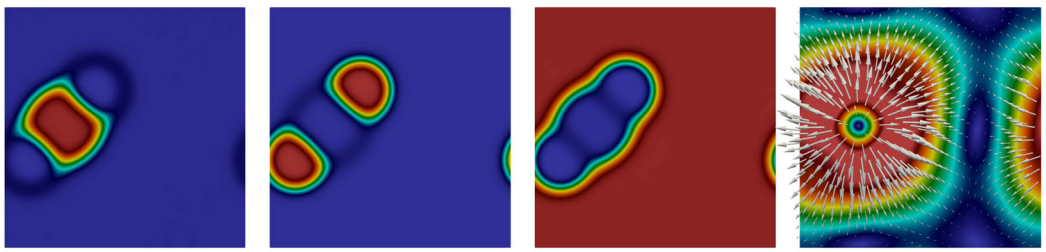

(c) $\bar{t} = 5.72 \times 10^{-4}$

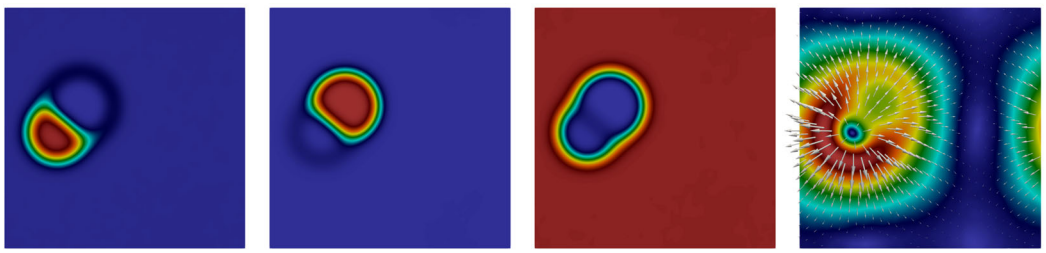

(d) $\bar{t} = 1.84 \times 10^{-3}$

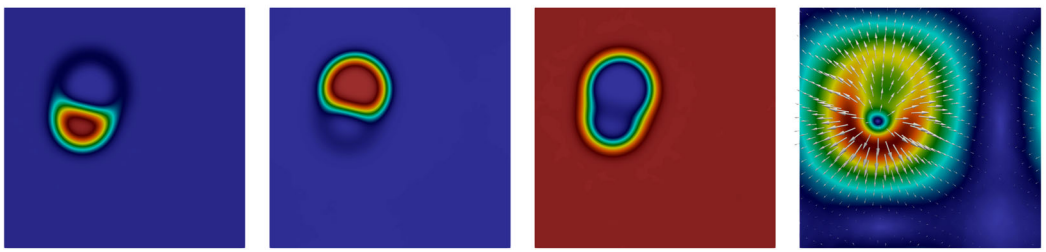

(e) $\bar{t} > 10^{-2}$

Fig. 3 Temporal evolution of the three phase fields together with the magnitude of the displacement vector and its direction

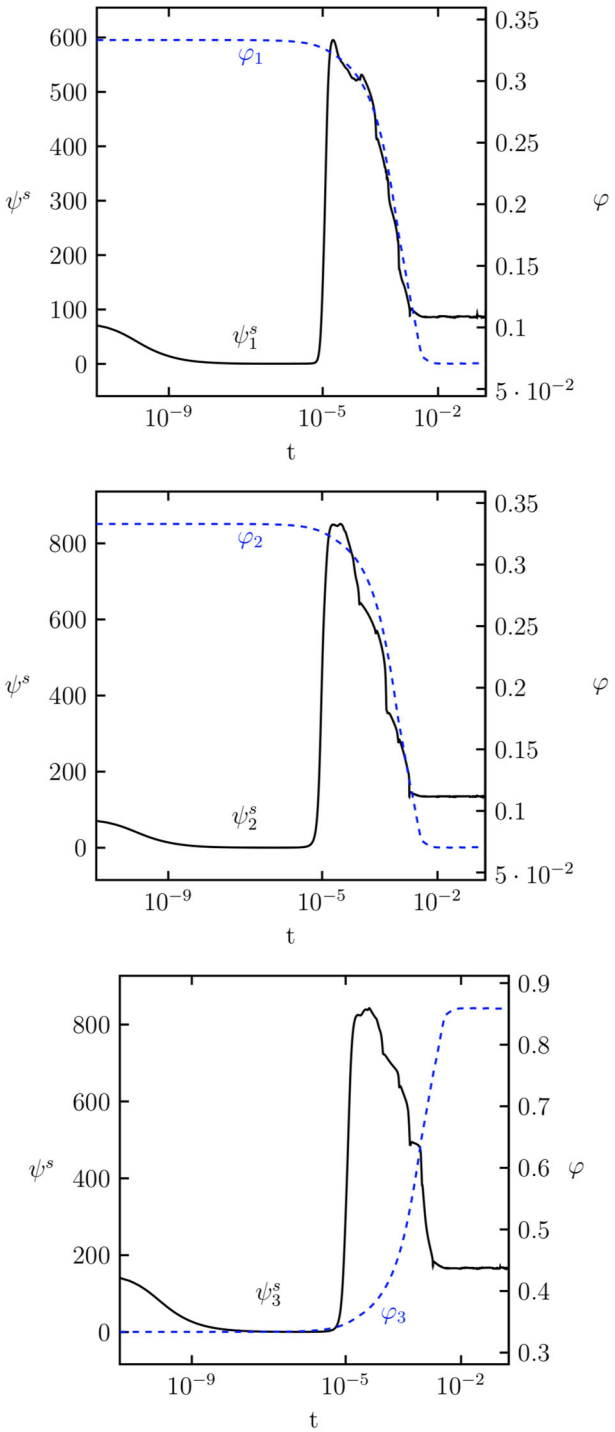

Fig. 4 Interfacial energies for phases $\mathcal{A}^1$, $\mathcal{A}^2$, and $\mathcal{A}^3$ along with their masses

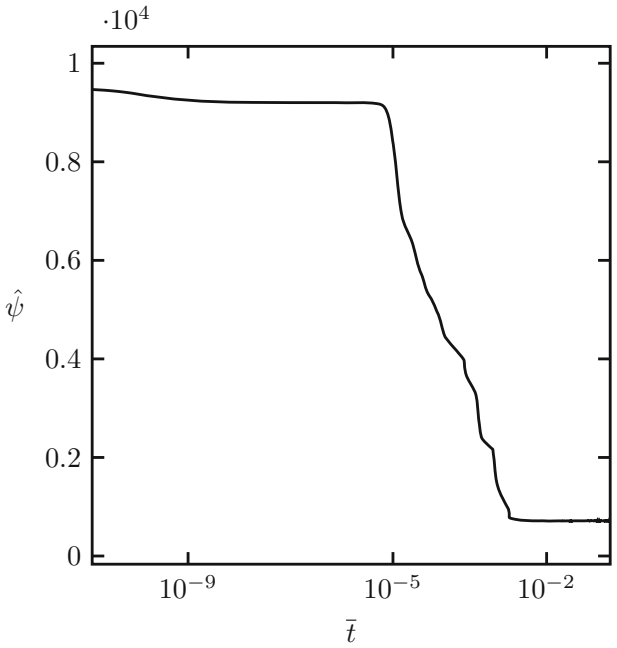

Fig. 5 During the whole evolution, the free energy is monotonically-decreasing

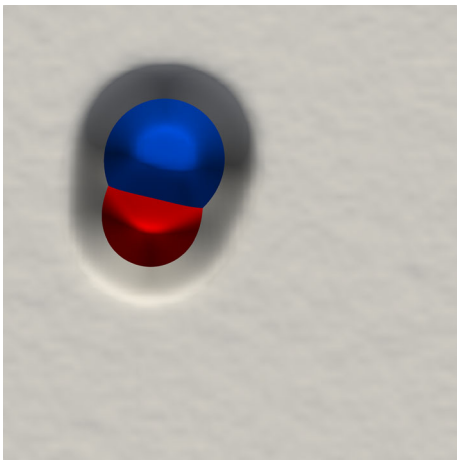

Fig. 6 Microstructural morphology of the ternary system at steady state $\bar{t} > \times 10^{-2}$

4.2 Ripening of spherical inclusions

We carry out a numerical simulation of a 3D configuration of three spherical inclusions. The spherical inclusions are composed of phases $\mathcal{A}^1$ and $\mathcal{A}^2$ while phase $\mathcal{A}^3$ serves as an interstitial phase. We study the stress-assisted volume changes triggered by the mass transport of the spherical inclusions associated with interfacial effects. We expect Ostwald ripening as a result of the differences in the size of the inclusions. We do not consider external contributions from body forces and external microforces. Consequently, we set $\mathbf{b} = \mathbf{0}$ and $\gamma^\alpha = 0$. Regarding the kinematics of the motion, the spatial velocity $\boldsymbol{v}$ is nearly constant as we do not take into account inertial effects during these quasi-steady processes. We do not allow for chemical reactions between the phases, and therefore, the reactions rates k_+ and k_- are zero. The latter entails that $s^\alpha = 0.0$. Hence, the stresses emerge solely from the mass transport associated with the interfacial interactions between the phases. Without loss of generality, the initial condition serves as the reference configuration. We choose this reference state as an undeformed configuration of the body. The initial and boundary conditions are given by

$$
\begin{aligned}
&S_1 = (x-0.25)^2 + (y-0.25)^2 + (z-0.25)^2 - 0.2^2,\\
&S_2 = (x-0.75)^2 + (y-0.75)^2 + (z-0.75)^2 - 0.1^2,\\
&S_3 = (x-0.75)^2 + (y-0.75)^2 + (z-0.3)^2 - 0.08^2,\\
&h = 0.2,\\
&\delta^1 = 0.31 - 0.8\left(0.5\tanh\left(\frac{S_1}{0.01h(h+2.0)}\right) + 0.5\right),\\
&\delta^2 = 0.31 - 0.8\left(0.5\tanh\left(\frac{S_2}{0.01h(h+1.0)}\right) + 0.5\right),\\
&\delta^3 = 0.31 - 0.8\left(0.5\tanh\left(\frac{S_3}{0.01h(h+0.8)}\right) + 0.5\right),\\
&\varphi_0^1 = 1 + \delta_1 + \delta_2,\\
&\varphi_0^2 = \delta_3,\\
&\varphi_0^3 = 1 - \varphi_0^1 - \varphi_0^2,\\
&\mathbf{u} = \mathbf{0},\\
&\text{in } \mathbf{P}, \text{ subjected to periodic boundary conditionson } \partial\mathbf{P} \times (0, T).
\end{aligned}
\tag{69}
$$

For the 3D numerical simulation in this section, we use the material parameters in Table 2. Nevertheless, we set the reaction rates $k_+ = 0$ and $k_- = 0$. As mentioned before, the phase $\mathcal{A}^3$ serves as an interstitial phase following the mass constraint given by (19). Figure 7a shows the initial condition for the phases distribution and displacements, respectively. The system of equations to solve is given by

$$\dot{\varphi}^1 = -\mathrm{Div}\, \boldsymbol{J}^1_{\mathrm{R}3}, \tag{70a}$$

$$\dot{\varphi}^2 = -\mathrm{Div}\, \boldsymbol{J}^2_{\mathrm{R}3}, \tag{70b}$$

$$\mathrm{Div}\, \mathbf{T}_{\mathrm{R}} = \mathbf{0}. \tag{70c}$$

where we use the phase $\mathcal{A}^3$ as the reference species. We solve the system of partial differential equation (70) in its primal form (66) and (68). We state the problem as follows: find $\{\varphi, \mathbf{u}\} \in \mathcal{C}^2(\mathbf{P})$ such that (61) subjected to periodic boundary conditions up to the second derivative of φ, and $\mathbf{u}$ with respect to $\mathbf{X}$ in a cubic open region $\mathbf{P} = (0, 1) \times (0, 1) \times (0, 1)$. We use the PetIGA [30] to solve the 64^3 element mesh of a polynomial degree 2 and continuity 1.

At early stages Fig. 7b, $\bar{t} < 1.182 \times 10^{-6}$, part of the phase $\mathcal{A}^1$ deposits on the surface of the inclusion $\mathcal{A}^2$ as a new spherical inclusion $\mathcal{A}^1$ of same radius appears. As the evolution proceeds, between the time range $1.182 \times 10^{-6} < \bar{t} < 2.79 \times 10^{-6}$, the inclusion of phase $\mathcal{A}^2$ becomes smaller as its mass goes into the solution. There is no deposition of phase $\mathcal{A}^2$ at this point in the evolution. Regarding the deformation, the stresses associated with the volume changes are small since the displacements do not change substantially (see Fig. 7c). Nevertheless, after $\bar{t} > 5.476 \times 10^{-6}$, rings composed of phases $\mathcal{A}^1$ and $\mathcal{A}^2$ appear around $\mathcal{A}^1$. This occurs as the solution gets supersaturated and the mass of phases $\mathcal{A}^1$ and $\mathcal{A}^2$ migrate to the surface of the more energetically stable structures in the system, which in this case correspond to the spherical inclusions (see Fig. 7d). Such mass transport induces volumetric stresses and concomitant displacements around the spherical inclusions (see Fig. 7d). As the system tries to minimise its free energy, the masses of phases $\mathcal{A}^1$, $\mathcal{A}^2$, and $\mathcal{A}^3$ in the solution separate and merge to form new spherical structures. The phase $\mathcal{A}^2$ locates around the spherical inclusions of $\mathcal{A}^1$. As mentioned before, the fact that the phases are diffusing induces volumetric stresses. Consequently, we see displacements where the phases are separating and merging (see Fig. 7d). Later on, $\bar{t} > 5.626 \times 10^{-3}$, the spherical inclusions composed of phase $\mathcal{A}^1$ and $\mathcal{A}^2$ merge to form a more energetically stable distribution of elongated structures (see Fig. 7e). Finally, the phase $\mathcal{A}^2$ wraps the phase $\mathcal{A}^1$, and $\mathcal{A}^3$ acts as an interstitial phase. The structure at steady state emerges as a result of the coupled chemo-mechanical interactions of the three-component system where the source of stress generation solely results from the mass transport of the phases (see Fig. 7e). Figure 8 shows the microstructural configuration at the steady-state.

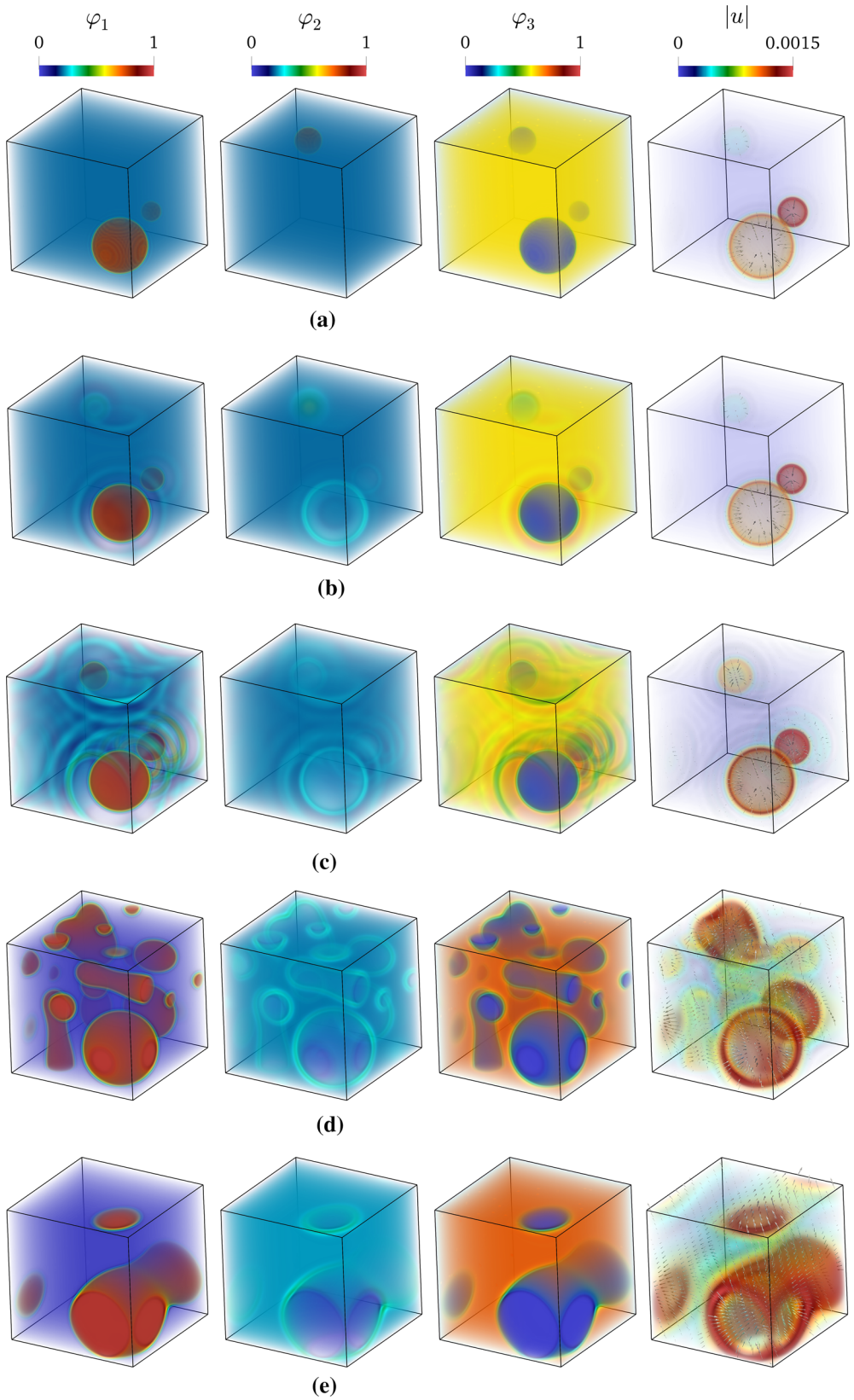

Fig. 7 The inclusions differ in size which drives the ripening process. The deformation will result from the mass transport of the phases as the smaller inclusions go into the solution and deposit in the surface of the larger inclusions

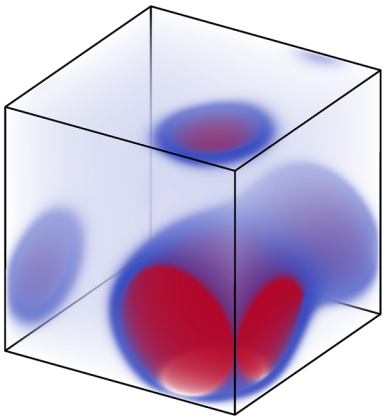

Fig. 8 Microstructural morphology at steady state for species concentration

5 Conclusions

We develop a thermodynamically consistent model that describes the evolution of chemically active mineral solid solutions. The theoretical foundations of the framework rely on modern continuum mechanics, thermodynamics far from equilibrium, and the phase-field model, which allow us to derive a set of coupled chemo-mechanical partial differential equations. Using 2D and 3D numerical simulations, we show the evolution of the stress-assisted volume changes triggered by mass transport and chemical reactions. We also include a constraint system using the Larché–Cahn derivative, which takes into account the mass constraint imposed by the solid crystalline structure. Finally, we conclude that the influence of mechanical effects upon chemically active mineral solid solutions must be taken into account and most importantly, they play a substantial role in the evolution of these geosystems.

Acknowledgements We are indebted to Professor Eliot Fried. We had many exhaustive discussions in which he gave us valuable ideas, constructive comments, and encouragement. This publication was made possible in part by the CSIRO Professorial Chair in Computational Geoscience at Curtin University and the Deep Earth Imaging Enterprise Future Science Platforms of the Commonwealth Scientific Industrial Research Organisation, CSIRO, of Australia. The European Union's Horizon 2020 Research and Innovation Program of the Marie Skłodowska-Curie grant agreement No. 777778. Lastly, we acknowledge the support provided at Curtin University by Curtin Combustion Centre, The Institute for Geoscience Research (TIGeR) and by the Curtin Institute for Computation.

Funding Open Access funding enabled and organized by Projekt DEAL.

References

1. Milke, R., Abart, R., Kunze, K., Koch-Müller, M., Schmid, D., Ulmer, P.: Matrix rheology effects on reaction rim growth i: evidence from orthopyroxene rim growth experiments. J. Metamorphic Geol. **27**(1), 71–82 (2009)
2. Tajčmanová, L., Vrijmoed, J., Moulas, E.: Grain-scale pressure variations in metamorphic rocks: implications for the interpretation of petrographic observations. Lithos **216**, 338–351 (2015)
3. Hobbs, B.E., Ord, A.: Does non-hydrostatic stress influence the equilibrium of metamorphic reactions? Earth-Sci. Rev. **163**, 190–233 (2016)
4. Moulas, E., Podladchikov, Y., Aranovich, L.Y., Kostopoulos, D.: The problem of depth in geology: when pressure does not translate into depth. Petrology **21**(6), 527–538 (2013)
5. Vrijmoed, J.C., Podladchikov, Y.Y.: Thermodynamic equilibrium at heterogeneous pressure. Contributions Mineral. Petrol. **170**(1), 10 (2015)

6. Wheeler, J.: Dramatic effects of stress on metamorphic reactions. Geology **42**(8), 647–650 (2014)
7. Zhong, X., Vrijmoed, J., Moulas, E., Tajčmanová, L.: A coupled model for intragranular deformation and chemical diffusion. Earth Planet. Sci. Lett. **474**, 387–396 (2017)
8. Gibbs, J.W.: ART.LII.—On the equilibrium of heterogeneous substances. Am. J. Sci. Arts (1820–1879) **16**(96), 441 (1878)
9. Gurtin, M.E., Fried, E., Anand, L.: The Mechanics and Thermodynamics of Continua. Cambridge University Press (2010)
10. Dal, H., Miehe, C.: Computational electro-chemo-mechanics of lithium-ion battery electrodes at finite strains. Comput. Mech. **55**(2), 303–325 (2015)
11. Miehe, C., Dal, H., Schänzel, L.-M., Raina, A.: A phase-field model for chemo-mechanical induced fracture in lithium-ion battery electrode particles. Int. J. Numer. Methods Eng. **106**(9), 683–711 (2016)
12. Tsagrakis, I., Aifantis, E.C.: Thermodynamic coupling between gradient elasticity and a Cahn–Hilliard type of diffusion: size-dependent spinodal gaps. Contin. Mech. Thermodyn. 1–14 (2017)
13. Larché, F., Cahn, J.W.: A linear theory of thermochemical equilibrium of solids under stress. Acta Metall. **21**(8), 1051–1063 (1973)
14. Larché, F., Cahn, J.W.: A nonlinear theory of thermochemical equilibrium of solids under stress. Acta Metall. **26**(1), 53–60 (1978)
15. Larché, F., Cahn, J.: Thermochemical equilibrium of multiphase solids under stress. Acta Metall. **26**(10), 1579–1589 (1978)
16. Gonzalez, O., Stuart, A.M.: A First Course in Continuum Mechanics. Cambridge University Press (2008)
17. Gurtin, M.E.: An Introduction to Continuum Mechanics, Vol. 158, Academic Press, 1982
18. Sedov, L.I.: A Course in Continuum Mechanics: Fluids, Gases and the Generation of Thrust, vol. 3. Wolters-Noordhoff (1972)
19. Gurtin, M.E.: Generalized Ginzburg–Landau and Cahn–Hilliard equations based on a microforce balance. Phys. D Nonlinear Phenomena **92**(3–4), 178–192 (1996)
20. Miranville, A.: Consistent models of Cahn–Hilliard–Gurtin equations with Neumann boundary conditions. Phys. D Nonlinear Phenomena **158**(1), 233–257 (2001)
21. Bonfoh, A., Miranville, A.: On Cahn–Hilliard–Gurtin equations. Nonlinear Anal. Theory Methods Appl. **47**(5), 3455–3466 (2001)
22. Cherfils, L., Miranville, A., Zelik, S.: The Cahn–Hilliard equation with logarithmic potentials. Milan J. Math. **79**(2), 561–596 (2011)
23. Clavijo, S., Espath, L., Calo, V.: Extended Larché–Cahn framework for reactive Cahn–Hilliard multicomponent systems, arXiv preprint (2021)
24. Cimmelli, V., Sellitto, A., Triani, V.: A generalized Coleman-Noll procedure for the exploitation of the entropy principle. In: Proceedings of the Royal Society of London A: Mathematical, Physical and Engineering Sciences, Vol. 466, The Royal Society, pp. 911–925 (2010)
25. Cahn, J.W., Hilliard, J.E.: Free energy of a nonuniform system. I. Interfacial free energy. J. Chem. Phys. **28**(2), 258–267 (1958)
26. Elliott, C.M., Garcke, H.: Diffusional phase transitions in multicomponent systems with a concentration dependent mobility matrix. Phys. D Nonlinear Phenomena **109**(3–4), 242–256 (1997)
27. Gurtin, M.E.: On a nonequilibrium thermodynamics of capillarity and phase. Q. Appl. Math. **47**(1), 129–145 (1989)
28. Evans, O., Spiegelman, M., Kelemen, P.: Phase-field modeling of reaction-driven cracking: determining conditions for extensive olivine serpentinization. J. Geophys. Res. Solid Earth (2020)
29. Singh, A., Pal, S.: Coupled chemo-mechanical modeling of fracture in polycrystalline cathode for lithium-ion battery. Int. J. Plast. **102636**,(2020)
30. Dalcin, L., Collier, N., Vignal, P., Côrtes, A., Calo, V.M.: PetIGA: a framework for high-performance isogeometric analysis. Comput. Methods Appl. Mech. Eng. (2016)
31. Balay, S., Abhyankar, S., Adams, M., Brown, J., Brune, P., Buschelman, K., Dalcin, L., Dener, A., Eijkhout, V., Gropp, W. et al.: PETSc users manual (2019)